7798–7819 *Nucleic Acids Research, 2023, Vol. 51, No. 15* *Published online 23 June 2023*
https://doi.org/10.1093/nar/gkad521

Spatially resolved transcriptomic analysis of the germinating barley grain

Marta Peirats-Llobet [1,†], Changyu Yi [1,†], Lim Chee Liew [1], Oliver Berkowitz [1,2], Reena Narsai[1], Mathew G. Lewsey[1,2,*] and James Whelan [1,2,3,*]

[1]Department of Animal, Plant and Soil Science, La Trobe Institute for Sustainable Agriculture and Food, School of Agriculture, Biomedical and Environmental Sciences, La Trobe University, Bundoora, Victoria 3086, Australia, [2]Australian Research Council Research Hub for Medicinal Agriculture, AgriBio Building, La Trobe University, Bundoora, VIC 3086, Australia and [3]Research Centre for Engineering Biology, College of Life Science, Zhejiang University, 718 East Haizhou Road, Haining, Jiaxing, Zhejiang 314400, China

Received February 22, 2023; Revised May 26, 2023; Editorial Decision May 27, 2023; Accepted June 03, 2023

ABSTRACT

Seeds are a vital source of calories for humans and a unique stage in the life cycle of flowering plants. During seed germination, the embryo undergoes major developmental transitions to become a seedling. Studying gene expression in individual seed cell types has been challenging due to the lack of spatial information or low throughput of existing methods. To overcome these limitations, a spatial transcriptomics workflow was developed for germinating barley grain. This approach enabled high-throughput analysis of spatial gene expression, revealing specific spatial expression patterns of various functional gene categories at a sub-tissue level. This study revealed over 14 000 genes differentially regulated during the first 24 h after imbibition. Individual genes, such as the aquaporin gene family, starch degradation, cell wall modification, transport processes, ribosomal proteins and transcription factors, were found to have specific spatial expression patterns over time. Using spatial autocorrelation algorithms, we identified auxin transport genes that had increasingly focused expression within subdomains of the embryo over time, suggesting their role in establishing the embryo axis. Overall, our study provides an unprecedented spatially resolved cellular map for barley germination and identifies specific functional genomics targets to better understand cellular restricted processes during germination. The data can be viewed at https://spatial.latrobe.edu.au/.

GRAPHICAL ABSTRACT

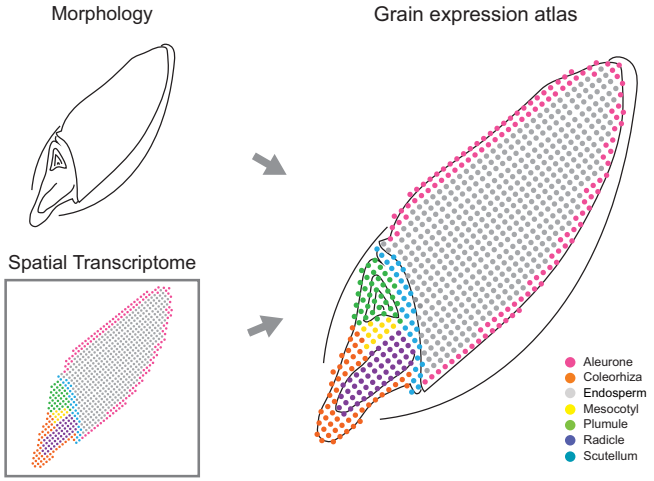

INTRODUCTION

Seeds provide 70% of human calorie intake and are essential for sustainable food security. This unique stage of the life cycle of flowering plants not only allows plants to optimise survival strategies, but has also formed the basis of settled human civilisation. Consequently, plants have been bred for seed yield and quality since the foundation of agriculture and the study of breeding continues intensively (1). While the genome sequence of agricultural crops greatly accelerates efforts to breed for desirable traits, it is the dynamic expression of the genome in the millions of cells that defines these traits. Thus, while whole-organ or tissue-specific transcriptome data is valuable in fundamental research and applications, recent technologies enabling the interrogation of gene expression at single-cell resolution have revolutionised

*To whom correspondence should be addressed. Tel: +86 17119366682; Email: jimwhelan@zju.edu.cn
Correspondence may also be addressed to Mathew G. Lewsey. Tel: +61 390327467; Email: m.lewsey@latrobe.edu.au
†The authors wish it to be known that, in their opinion, the first two authors should be regarded as Joint First Authors.

our ability to understand plant growth and function at the basic level of organisation, i.e. the cell (2).

Several approaches to obtain single-cell transcriptomes have been developed, with microfluidics-based single-cell sequencing (scRNA-seq) currently of wide use due to the high-throughput nature of this technology. The first scRNA-seq studies in plants were applied to root tissues (3–5) because of their spatially defined developmental profile along the longitudinal axis and the relative ease of isolating individual cells. scRNA transcriptomes are also emerging for other organs, showing that this approach can be successfully applied to a variety of tissues (6–9).

It has been proposed that the plant science community come together around the goal of creating a complete plant cell atlas, which should incorporate transcriptomic information about all cells in an entire plant (10). scRNA-seq is considered a foundational technology for this goal, but the technology has limitations that prevent it being a full solution for the plant cell atlas. Some cell populations or types may not be assayed in scRNA-seq experiments, due to the varying size of plant cells, different cell wall compositions, the necessity and difficulty of optimising protoplast or nuclei isolation methods for individual tissue types, the requirements for substantial amounts of input tissue, and the relative rarity of certain cell types. Moreover, scRNA-seq requires the dissociation of tissues into individual cells for microfluidic handling. This discards crucial information on the spatial origin of those cells, which defines their identity and function. As a result, scRNA-seq data analysis reconstructs cell identities and defines cell developmental trajectories by relying on cell-type-specific marker genes and gene co-expression. These approaches are bioinformatically challenging and may introduces biases (4,11,12).

Spatial transcriptomics is an emerging approach in plant biology that promises to overcome some of the limitations of scRNA-seq (13,14). This approach can be applied to any plant tissue that can be sectioned and morphology maintained, which has occurred extensively for many crop plants. When sectioning is optimised, it requires small amounts of tissue, employs fixation to preserve a full snapshot at a particular time, and retains cell spatial information, which are all very attractive qualities. These indicate spatial transcriptomics could make a significant contribution to obtaining cell-specific transcriptomes in plants, complementing scRNA-seq approaches and opening an exciting era for plant biology.

Few spatial transcriptomic studies have been reported in plants, contrasting with mammalian systems where these technologies have been successfully applied to gain insights into development and disease progression (15,16). The first plant spatial transcriptomic study used a 100 μm resolution array to demonstrate the applicability of the method on the *Arabidopsis thaliana* inflorescence meristem, *Populus tremula* leaf buds and *Picea abies* female cones (17). A second study that used a different technology, Stereo-seq, with a 220 nm bead size and resolution depending on the numbers of beads that are 'binned', detected almost 20 000 expressed genes. Here, subtle differences were revealed in the expression of genes associated with photosynthesis across the *Arabidopsis* leaf cells. However, the authors noted that some cells associated with vascular bundles were missing (18). A gene expression map of flower development in orchids (19) and an atlas to study vascular tissue development in poplar (20) were both generated using the 10× Genomics Visium technology at 55 μm resolution. This technology was also used to confirm the laser microdissection description of the spatial integration of C4 and CAM photosynthetic metabolism (21). Most recently, researchers combined Multiplexed Error-Robust Fluorescence *in situ* Hybridization (MERFISH) and slide-seq spatial technologies to validate newly discovered marker genes and aid in cluster annotation of complex organs such as germinating *Arabidopsis* seeds and siliques (22). A combined approach using single-nuclei RNA-seq, BGI single-cell Stereo-seq, 10x Visium spatial RNA-seq and BMKMANUS1000 RNA-seq has also been used to profile tomato callus during shoot regeneration, revealing callus displays a high level of cellular heterogeneity and that the shoot primordia originates from the sub-epidermis (23).

Here, we present a time-series spatial transcriptomic analysis of germinating barley grain at 55 μm resolution. We detected the expression of >14 000 genes over five to six tissue types, at 0, 1, 3, 6 and 24 h after imbibition (HAI). We analysed and distinguished the discrete spatial and temporal transcriptional activity between barley grain tissues and between domains within tissues. This allowed us to analyse the distinct and subtle expression domains of individual gene family members, for ion and auxin transporters, genes encoding proteins involved in transcription and translation, starch degradation, and relate them to specific spatial functions. This spatial and temporal resolution in gene expression will provide specific targets for grain improvements and promoters to drive precise expression for synthetic biology approaches to alter grain quality.

MATERIALS AND METHODS

Spatial transcriptomics tissue preparation

Plant growth and tissue preparation. Barley grains (cv La Trobe) were surface sterilized using the chlorine-gas method in a fume hood, germinated on top of two layers of sterilized filter paper with 12 ml of sterile water added and wrapped with foil at 23°C. Seeds were harvested at 0, 1, 3, 6 and 24 HAI.

Grain sectioning. The seeds for the Visium experiment were collected at the indicated time-points and hand-dissected longitudinally. The seeds were immediately snap frozen in an isopentane bath (2-methylbutane, Sigma Aldrich, cat no. 270342-1L) for 1 min, subsequently embedded in Optimal Cutting Temperature (OCT, Tissue-Tek, cat no. 4583) and the blocks frozen in an isopentane bath and kept on dry ice. The cryoblocks were cut on a cryostat (Leica Biosystems; MA, USA) to a thickness of eight μm at –18°C. The sections were carefully place on a prechilled Tissue Optimization (TO) or Gene Expression (GE) slide and kept frozen at –80°C until required.

Fixation, staining and imaging. The slides were dried on a metal plate (PN-1000317, 10x Genomics) in the thermocycler at 37°C for 1 min, fixed with chilled methanol at –20°C

for 30 min, stained with 0.1% (w/v) Safranin O (Sigma-Aldrich, cat no. S8884-25G) in 50% (vol/vol) Ethanol with 2 U/μl RNase inhibitor at room temperature (RT) for 5 min and washed in increasing concentrations of EtOH until the discarded liquid was clear. After drying at 37°C for 1 min, the slides were mounted in 85% (v/v) glycerol + 2 U/μl RNase inhibitor, covered with a coverslip and images of sections were taken using Axio-Imager.M2 microscope (Zeiss). TO slides were captured in on image while GE slide capture areas were imaged individually. Raw images were stitched together using Zen blue software v2.5 (Zeiss). Prior to imaging, the microscope settings were validated using the Visium Imaging Test Slide (PN-2000235). The optimised settings were saved into the TO macro for following experiments. After imaging, the coverslip was removed immediately, and the slide immersed at 45° angle in 3× SSC buffer and washed once with 3× SSC buffer before air drying.

Tissue pre-permeabilization, permeabilization and reverse transcription. To pre-permeabilize the tissue, the slides were mounted in a plastic cassette and sections incubated in pre-permeabilization solution (24) (48 μl Exonuclease I buffer, NEB, cat no. B0293S; 4.5 μl of BSA, Sigma-Aldrich, cat no. A7039-100G; and 2% (w/v) PVP40, Sigma-Aldrich, cat no. PVP40-1KG) at 37°C for 30 min. This was followed with a wash with 0.1 × SSC buffer (Sigma-Aldrich, cat no. S6639L). The sections were permeabilized with Permeabilization mix™ (10x Genomics) at 37°C for different times (1, 3, 6, 15, 30 min TO slides) or for 3 min (GE slides). Then, wells were washed with 0.1× SSC buffer. After permeabilization, Reverse transcription mixture™ (10x Genomics) was added to each section and incubated at 56°C for 45 min as described in the 10x Genomics User guide (PN-1000186, CG000239_VisiumSpatialGeneExpression_UserGuide_RevD).

Tissue removal and washes (TO slide only). To remove the tissue, a hydrolytic enzyme mixture was prepared by adding 70 μl of each enzyme (Supplementary Table S1); cellulase (Yakult -'ONOZUKA' R-10, cat no. YAKL0012), pectate lyase (Megazyme, cat no. E-PCLYAN2), xyloglucanase (Megazyme, cat no. E-XEGP), endo 1,4 β-xylanase (Megazyme, cat no. E-XYNACJ), endo 1,4 β-mannanase (Megazyme, cat. no. E-BMACJ) and lichenase (Megazyme, cat. no. E-LICHN) to 140 μl of 250 mM sodium citrate buffer (Sigma-Aldrich, cat. no. 71497-250 G), pH 6.6. The enzymatic mixture was added to the wells and incubated in a Thermo Mixer at 37°C for 90 min with shaking (300 r.p.m.). The wells were washed with 0.1× SSC buffer. Samples were incubated with 10% (v/v) Triton X-100 solution in a Thermo Mixer at 56°C for 1 h with shaking (300 r.p.m.), followed by a wash with 0.1× SSC buffer. Next wash consisted in a mixture of RLT buffer (Qiagen ref.79216) with 1% (v/v) β-mercaptoethanol, which was incubated in a Thermo Mixer at 56°C for 1 h with shaking (300 r.p.m.) and followed by a wash with 0.1× SSC buffer. A final incubation with 70 μl proteinase K mixture (60 μl of proteinase K (Qiagen, cat. no. 19131) and 420 μl of PKD buffer (Qiagen, cat no. 1034963) was performed in a Thermo Mixer at 56°C for 1 h with shaking (300 r.p.m.). Hybridization chamber was detached, and the slide washed in a petri dish with 50°C pre-warmed wash buffer 1 (2× SSC/0.1% SDS) at 50°C for 10 min with shaking (300 rpm). The slides were further washed with wash buffer 2 (0.2× SSC) and wash buffer 3 (0.1× SSC) at RT for 1 min with shaking (300 rpm). The slide was spin-dried in a swing-bucket centrifuge.

Fluorescence imaging or library preparation, and sequencing. When using the Tissue Optimization workflow, a fluorescent image (mRFP filter, Excitation: 559/85 Emission: 600/90) of the cDNA footprint was taken. The whole slide was recorded using a Plan-Apochromat 10×/0.45 M27 objective and the tiling function of the Axio-Imager.M2 microscope (Zeiss). The final file included each of the eight capture areas, 8 × 8 mm (the fiducial frame and the capture area); with the microscope set to ∼1–2 mm beyond the fiducial frame for optimal image alignment. The capture resolution was 0.454 μm/pixel. Raw images were stitched together using Zen blue software v2.5 (Zeiss). When following the Gene Expression workflow, libraries from the different capture areas were synthesized as described in 10x Genomics User guide (PN-1000190, CG000239_VisiumSpatialGeneExpression_UserGuide_RevD).

Visium libraries were sequenced on an Illumina NextSeq 550 platform according to the 10× Genomics Visium manufacturer's instructions (NextSeq 500/550 High Output kit v2.5 (150 cycles) 20024907, CG000239_VisiumSpatial GeneExpression_UserGuide_RevD), targeting 100 million reads using dual indexing kit TT set A (PN-1000215, 10x Genomics).

Visium spatial gene expression analysis

Imaging and data processing. Images of the bright field sections were loaded into Loupe browser software (10x Genomics) and the fiducial frames were manually adjusted. The resulting loupe files were used for downstream analysis.

Spatial transcriptomics data processing. Selection of spots and image alignment was performed in Loupe Browser (v. 6.2.0, 10x Genomics) to generate alignment files for each section. The sequencing data, bright field images and alignment files were used as input for the Space Ranger (v. 1.3.1, 10× Genomics) to generate gene-spot matrices. IBSCv2 barley genome assembly was used as the reference genome for Space Ranger (25). For each section, spots with a total UMI count <30 and <10 expressed genes were excluded from the following analysis. For each time point, the data from four sections were merged with the "merge" function from Seurat package (v. 4.1.0) and normalized using SCTransform (settings: variable.features.n = NULL, variable.features.rv.th = 1) (11). Section variability within the data were regressed out using the 'vars.to.regress' function from SCTransform. Principal component analysis (PCA) was performed on the genes with residual variance >1, and the 30 most significant components were retained as input for Uniform Manifold Approximation and Projection (UMAP) (11) and for spot clustering. Generation of spot clusters was made using the 'FindNeighbors' (settings: reduction = 'pca', dims = 1:30) followed by the 'FindClusters' functions in Seurat, where the default algorithm was used

to construct a Shared Nearest Neighbor (SSN) graph and apply the Louvain algorithm for cluster generation. Cluster resolution was set from 0.4 to 0.8. The identity of the clusters was assigned based on their location in the section according to the morphology of a barley grain. To identify marker genes for each cluster, pair-wise comparisons of individual clusters against all other clusters were performed using the 'FindAllMarkers' function (settings: min.pct = 0.05, logfc.threshold = 0.25, only.pos = T) with Wilcoxon rank sum test in the Seurat package. The marker genes were further filtered with an adjusted P value < 0.05 (11).

Orthology analysis. *Arabidopsis* and rice orthologues to barley genes were identified using the genome pair orthology tool (OMA browser - https://omabrowser.org/oma/genomePW/) (26). Note that many of the genes were many to many orthologues, but only those within the set that were orthologous to the genes in our subset are shown. For the rice genes, the identifiers were converted from RAP to MSU identifiers for the Genevestigator analysis, whereby mRNA-seq data from various rice tissues were examined for the marker genes expressed in at least 4 time points, in each tissue.

Temporal and spatial specific analyses. Marker genes of each cluster identified at 0, 1, 3, 6 and 24 HAI were matched to all the genes in the genome and re-organised such that the marker genes in each of the time points in each of the tissues can be compared across rows. This revealed that 1412 genes were identified as marker genes in at least one tissue in at least one time point. In order to unveil any biological processes that may be specific to a tissue, the gene descriptions for each time point for each tissue (25 input sets) were independently examined using a wordcloud generator (https://monkeylearn.com/word-cloud/) to identify the terms occurring multiple times. Note, the words 'protein', 'superfamily' and 'family' were first removed to avoid bias. Outputs were returned as tables containing terms and number of occurrences for that term in each set. The outputs were then filtered keeping only the terms that were present in the gene-sets from at least three time points for a given tissue or contained five or more genes with that term i.e. spatial expression. Similarly, the terms that were present in the gene-sets from the same time point across at least three tissues were kept i.e. temporal specific expression. In this way, 26 functional descriptions/categories were identified.

Identification of spatially variable genes and co-expression gene modules. Spots that annotated as embryo tissues were identified for each time point and their expression data normalized using SCTransform as described above (11). For each section, spatial information between the spots were represented by an adjacency weight matrix which was calculated using the spot coordinates and Moran's I spatial autocorrelation statistics were computed using the normalized expression data along with associated spatial adjacency weight matrix using the MERINGUE framework (27). SVGs were defined as Moran's $I > 0.25$, adjusted P value <0.01, expressed in $>5\%$ spots in a section, and at least two sections for a time point were considered as for that time point. hdWGCNA was used to perform co-expression analysis for 24 HAI SVGs (28) using a signed network and 'bicor' correlation. Module detection was performed with default settings, and the minimal module size was set to 50 genes. After module detection, highly correlated modules were merged using a tree cut height of 0.45. For each module, an eigengene, which is defined as the first principal component of the module's expression pattern, was calculated. The intra-modular connectivity (kME) was calculated using the SignedKME algorithm for each gene, which represents its correlation with the module eigengene value. Gene ontology (GO) annotation of barley were retrieved from Shiny GO database (Version 0.75) (29) and GO enrichment analysis was performed with the clusterProfiler package (30). Overrepresentation of GO terms in the category 'biological process' was identified by hypergeometric distribution.

Spatial transcriptomics validation

RNA in situ hybridisation. Seeds were cut longitudinally to equal half and fixed in ice-cold farmers fixative (3:1 ethanol:acetic acid). Samples were placed in the cold room (4°C) overnight. The fixed tissue was dehydrated using the Leica Semi-Enclosed Benchtop Tissue Processor TP1020 (Leica Biosystems, Mount Waverley, Australia) at room temperature in a graded series of ethanol (1 h each 75%, 85%, 100%, 100% and 100% v/v) using vacuum. The tissues were then shifted to a graduated ethanol:xylene series (80 min in 75%:25%, 50%:50%, 25%:75% v/v), finished with a xylene series (100% (v/v) twice for 1 h) and vacuum. Tissue was then added to molten Surgipath Paraplast® Paraffin (Leica Biosystems) at 65°C and vacuum for 2 h. Paraplast blocks were then prepared with half seed in each block using the Leica Heated Paraffin Embedding Module EG1150 H with the added Leica Cold Plate for Modular Tissue Embedding System EG1150 C (Leica Biosystems). Embedded tissues were cut at eight μm sections and *in situ* hybridization was carried out according to modified protocol from (31) using 50°C hybridization temperature and 0.2× SSC washes. Gene of interest was amplified using designed primers (Supplementary Table S2) and cloned into pGEMT-Easy vector (Promega). Using the DIG RNA Labelling Kit (Roche Diagnostics), Digoxigenin-labelled antisense and sense RNA probes were transcribed from T7 or SP6 promoter of pGEMT-Easy vector (Promega) according to manufacturer's instructions. All hybridization results were observed and photographed using a Zeiss Axio Observer A1 microscope (Carl Zeiss AG).

RESULTS

Establishing a spatial transcriptomics workflow for barley grains

To obtain the transcriptional signature of barley grains from thinly sliced sections whilst preserving spatial information, we optimised spatial transcriptomics using Visium technology (10x Genomics) for germinating barley grains (0, 1, 3, 6 and 24 HAI) (Supplementary Figure S1a). The grains were cut in half, snap-frozen in an isopentane bath and embedded in optimal cutting temperature to generate

cryoblocks (Supplementary Figure S1b). We prepared eight μm thick longitudinal sections of the barley grains, then mounted them onto the active sequencing areas of Visium Gene Expression slides (6.5 × 6.5 mm^2, 10x Genomics, Supplementary Figure S1b). These active areas contain ∼5000 spot arrays with a diameter of 55 μm and a centre-to-centre distance of 100 μm (Supplementary Figure S1c). The spots on these slides are coated with spot-specific positional barcodes attached to oligo (dT) primers and unique molecular identifiers (UMIs) used for locating, capturing, and identifying the mRNAs, respectively (see methods and Supplementary Figure S1). In total, we prepared and analysed 20 samples, i.e. four sections per grain for each of the five time points (Supplementary Figure S1b). To assess whether the detected transcript signal was stringently confined under individual plant cells, we used the Visium Tissue Optimization kit (10x Genomics) with modifications to suit barley grains (see methods and Supplementary Figure S2, adapted from (24). To further determine the optimal conditions for the starchy barley grain, we compare the sequencing quality of a pre-permeabilization method described in (24) and the standard permeabilization method (10x Genomics) using sections from two different seeds at the 24 HAI time point. A similar number of genes (c. 13 000) was detected in all six of these sections (Supplementary Figure S2e) leading to the use of the standard permeabilization method for all subsequent gene expression experiments given its faster processing time.

Spatiotemporal gene expression dynamics during barley grain germination

We applied the optimised spatial transcriptomics workflow to study spatiotemporal gene expression dynamics during barley germination in an unbiased manner. We collected grains across a time-series of 0 (dry), 1, 3, 6 and 24 HAI and obtained four serial sections (per time point) along their longitudinal axis. Space Ranger (10x Genomics) was used for primary data processing and gene expression data overlaid upon grain section images using Loupe Browser. Among all sections, the minimum number of spots covered by tissue is 1171 and the highest number of tissue-covered spots is 1858. Within those tissue-covered spots, the mean number of reads per spot ranges from 57 397 to 103 993. The median UMI counts per spot varied between 69 to 1689 with median genes per spot between 57 and 1092 across the different sections. (Supplementary Figure S3, Supplementary Table S3). Note that the embryo tissues show much higher UMI and gene numbers (Supplementary Figure S4, Supplementary Figure S5). Secondary analysis used Seurat and SCTransform to generate clusters across four sections for each time point with the uniform manifold approximation and projection (UMAP) algorithm for dimensionality reduction (32,33). Resulting outputs for 24 HAI are shown in Figure 1A–D and for all other time points in Supplementary Figures S6, S7, S8 and S9 for 0 HAI, 1 HAI, 3 HAI and 6 HAI, respectively. A total of 11 clusters were identified at 24 HAI based on histological features and spatial transcriptomic data, with one cluster each for the coleorhiza, scutellum and aleurone, three for the embryo and five for the endosperm (Figure 1A, B, Supplementary Figure S10). The four sections showed high correlation with a Pearson correlation coefficient from 0.89 to 0.96 at 24 HAI (Figure 1C, D), and the high correlation across sections were also observed at other time points (Supplementary Figure S11). Furthermore, the four sections showed a similar proportion of number of spots (Supplementary Figure S12) and a high correlation (Supplementary Figures S13–S17) for clusters at each time point. These results again showed the high reproducibility across different sections. Marker genes for each tissue/cluster were identified by comparison to their expression in all other clusters at all time points (Supplementary Table S4).

We compared our spatial transcriptomic analysis to a published tissue-specific transcriptome analysis of barley grains generated by hand dissection to determine how closely the two approaches agreed with each other (34). The tissue-specific analysis detected expression of 19 611 genes across all tissues, compared with 14 594 genes detected across our complete spatial transcriptomic dataset (Figure 1E). Expression was next benchmarked per tissue. The spatial transcriptomic approach consistently detected between 83% and 90% of expressed genes present in the same tissue of the tissue-specific RNA-seq experiment, except for in the endosperm (Figure 1E). Spatial transcriptomics detected twice as many expressed genes in the endosperm than tissue-specific RNA-seq, but with almost all the expressed genes detected by hand dissection also present in the spatial transcriptomic dataset (Figure 1E). Note that the spatial transcriptomic data presented here comprises four sections of eight μm thickness each along the longitudinal axis of a grain that is around 5000 μm wide. Therefore, in comparison to tissue-specific sequencing only a portion of the whole grain will have been sampled which might not include all cell types. Correlations of gene expression across the different time points between the embryo, scutellum and aleurone of the spatial transcriptomics and the tissue-specific RNA-seq were R^2 ranging from 0.42 to 0.59. For the endosperm, no correlation was observed with R^2 between 0.09 and 0.16 (Supplementary Figure S18). In bulk RNA sequencing the expression of a gene is averaged over thousands to millions of cells, and the expression can represent a high abundance in a few cells or uneven expression levels, which remains unresolved following Simpson's paradox (35). Based on these benchmarks, spatial transcriptomics on barley grain is comparable in depth to tissue-specific sequencing with the added advantage of spatial resolution that eliminates any potential errors that arise due to averaging of expression levels that may be present in a cellular landscape (36).

Sets of expressed marker genes which were defined by comparing gene expression of different clusters pair-wisely (see methods) could be clearly defined for each cluster, which corresponded to individual tissues or regions within tissues, at 24 HAI (Figure 2A). Again, we detected a higher number of UMIs and genes in the embryo tissues (Supplementary Figure S19, Supplementary Figure S20). In coleorhiza (cluster col-1) expression of a distinct set of four genes was observed, with a second set that overlapped the radicle (cluster emb-3) (Figure 2A, Supplementary Table S5). The latter is not unexpected given the relationships between radicle and coleorhiza. The scutellum (cluster scu-1)

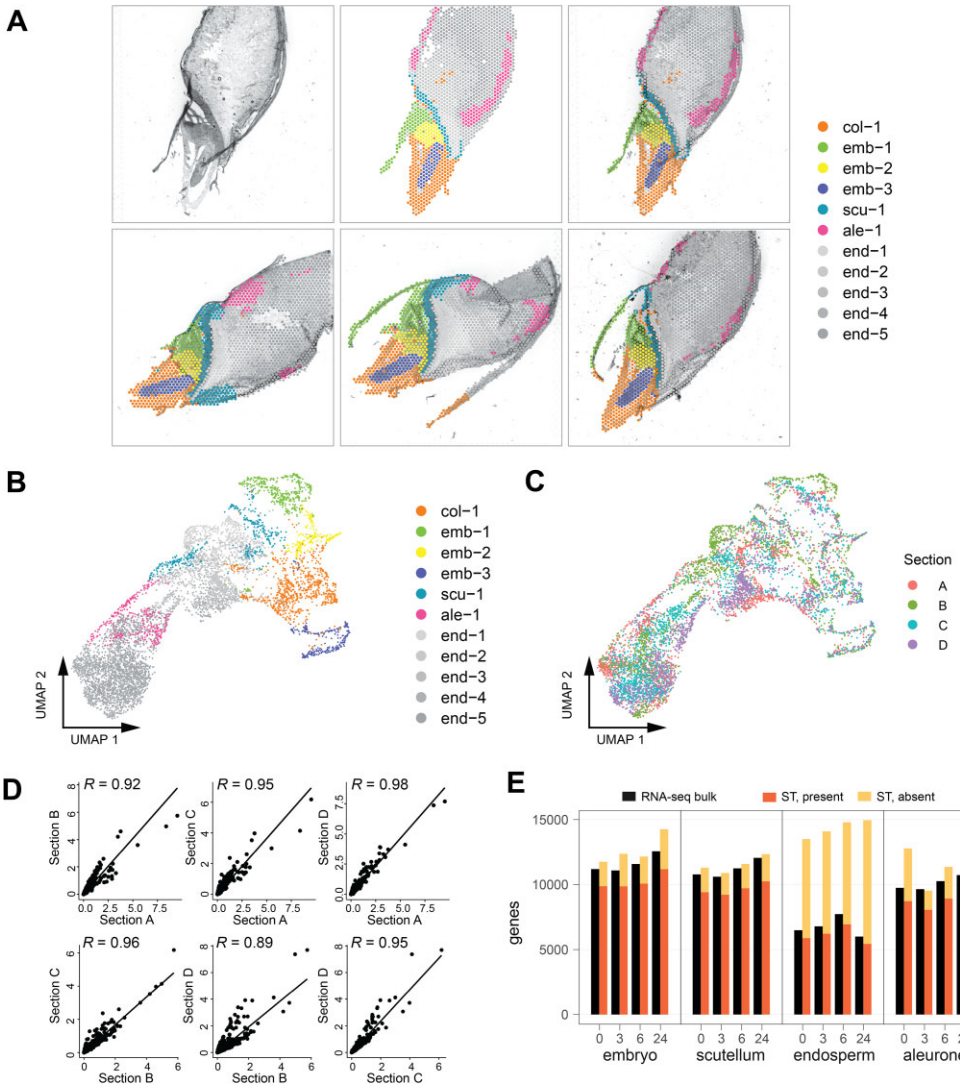

Figure 1. Spatially resolved transcriptome analysis of barley grain. (**A**) Spatial visualization of the unbiased spot clustering for four 24 h after imbibition (HAI) barley sections. Top left panel, bright field image of section #1, top middle panel, spatial localization of each cluster of section #1, top right panel, merged bright field image and spatial clusters of section #1. Bottom panels, merged bright field image and spatial clusters of other three sections. The tissue/cell-type identity of each cluster was assigned based on the location of each cluster. Col: coleorhiza, emb: embryo, scu: scutellum, ale: aleurone, end: endosperm. (**B**) Uniform manifold approximation and projection (UMAP) of spatial spots from four 24 HAI barley sections. Dots correspond to individual spots on the Visium slide; $n = 6961$ spots; colours indicate cluster association for each spot. (**C**) UMAP of spatial spots from four 24 HAI barley sections. Colours indicate different sections for each spot. (**D**) Pair-wise Pearson correlation between different sections for 24 HAI. Dots correspond to genes expressed in at least 5 spots. X axis and Y axis show the average of normalized count of tissue covered spots from two different sections, respectively. Pearson correlation coefficient is indicated as *R*. (**E**) Number and overlap between genes detected by bulk RNA-seq of barley grain tissues and spatial transcriptomics. For genes identified by spatial transcriptomics, their presence or absence in the same location as in a tissue-specific bulk RNA-seq experiment (34) was determined. The bar chart indicates the number of genes across comparable time points and tissues between both experiments. The cut-offs for inclusion in this comparison were at least five transcripts per million (TPM) for the RNA-seq experiment and at least five UMI per million for the spatial transcriptomics data, respectively.

expressed a distinct set of marker genes as well as some additional marker genes that overlapped with the endosperm, which is again not unexpected. The embryo was divided into three clusters. Of these, the coleoptile (cluster emb-1) expressed a distinct set of marker genes, whilst the radicle (cluster emb-3) and mesocotyl (cluster emb-2) expressed some overlapping marker genes that were differentiated by magnitude of expression. The endosperm was partitioned into five clusters, that could not be distinguished from one another by small sets of marker transcripts. It is therefore likely that the endosperm clusters arose from more complex or subtle differences in gene expression patterns. These five clusters may reflect differential water uptake and mobilisation of reserves across the endosperm upon imbibition, demonstrating the spatial heterogeneity in the magnitude of expression of genes between cells in the same tissue. Considered together, these results demonstrate the advantage of the spatial transcriptomic approach. It allows tissues and regions within tissues to be distinguished by a combination of their physical location and gene co-expression,

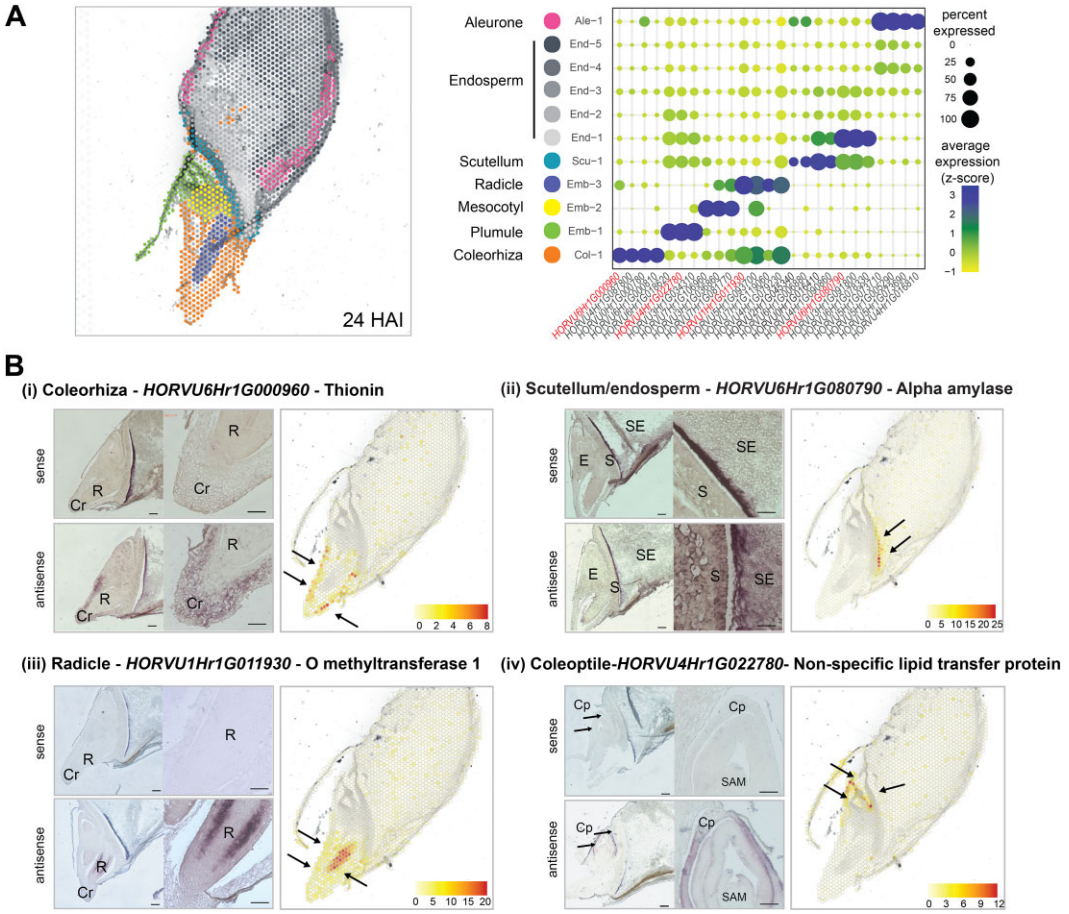

Figure 2. Identification of tissue-specific marker genes and their validation by *in situ* hybridisation. (**A**) Spatial representation of the 11 clusters determined at the 24 HAI timepoint (left panel) and bubble plot (right panel) showing transcript enrichment (average expression and percentage) of representative cell type-specific marker genes in the 11 clusters. Spot colours correspond to the same tissues in the bubble plot. Genes highlighted in red were validated by *in situ* hybridisation. (**B**) *in situ* hybridization of selected marker genes (i) *HORVU6Hr1G000960*; (ii) *HORVU6Hr1G080790*; (iii) *HORVU1Hr1G011930*; (iv) *HORVU4Hr1G022780* confirmed localization of tissue-type specific transcripts at 24 HAI timepoint. For each *in situ* hybridisation, top panels show hybridisation with the sense probes (negative controls) and bottom panels with the antisense probes. *In situ* images on the right correspond to 40x magnifications of images on the left. Scale bars correspond to 200 μm and colour scales represent normalised counts. Coleorhiza (Cr, Col), Radicle (R), Coleoptile (Cp), Shoot apical meristem (SAM), Aleurone (A, Ale), Starchy endosperm (SE, End), Embryo (E, Emb), Scutellum (S, Scu). Black arrows indicate the expression areas.

rather than by co-expression alone. We were consequently able to manually assign and curate spot locations to tissues without solely relying on marker genes or bioinformatic algorithms.

Validation of spatial expression by RNA *in situ* hybridisation

The expression patterns of transcripts detected by spatial transcriptomics were orthogonally validated using RNA *in situ* hybridisation (Figure 2B). *THIONIN* genes encode low molecular weight basic cysteine-rich antimicrobial peptides and are highly expressed early in germination in a tissue-specific manner in rice coleoptiles (37). Spatial transcriptomic analysis at 24 HAI indicated a coleorhiza-specific expression pattern for a *THIONIN* gene (*HORVU6Hr1G000960*) (Figure 2B, i). This was confirmed by RNA *in situ* hybridisation (Figure 2B, i). Alpha-amylases are critical enzymes for the mobilisation of starch reserves in germinating barley grains and have a scutellum and aleurone expression pattern (38). Spatial transcriptomics detected *HORVU6Hr1G080790* gene expression in the scutellum at 24 HAI, with strongest expression at the ventral end (Figure 2B, ii). RNA *in situ* hybridisation confirmed a scutellum expression pattern but could not distinguish expression magnitude across the scutellum. Any localised gradient in expression is difficult to resolve by RNA *in situ* hybridisation due to the non-linear nature of colorimetric detection methods that are end-product inhibited. For the radicle, the specific expression of an *O METHYLTRANSFERASE 1* gene (*HORVU1Hr1G011930*) involved in lignin biosynthesis was confirmed (39) (Figure 2B, iii). Coleoptile and leaf specific expression of a gene encoding a non-specific lipid transfer protein (*HORVU4Hr1G022780*) has been previously reported in barley (40,41). A similar pattern was observed here by RNA *in situ* hybridization and spatial transcriptomics (Figure 2B, iv).

Thus, the spatial transcriptomics results for germinating barley grain were consistent with the localisation,

abundance and depth obtained with other approaches, but had the advantage of combining all data into a single high-throughput approach.

Conservation of spatial expression patterns across species

Given the extensive transcript profiling studies in *Arabidopsis* tissues we undertook an orthology approach to determine if the marker genes defined in this study also displayed tissue specific expression in *Arabidopsis*. Orthologs were defined in *Arabidopsis* for the top 10 genes per cluster based on specificity, per time point, using OMA (26). This identified 14 *Arabidopsis* genes for endosperm, 25 genes for aleurone, 44 genes for scutellum and 145 genes for embryo. Note that most genes have a many-to-many relationship in each orthogroup, but paralogs were not included in this number. Analysis of the tissue expression pattern for these genes using Genevestigator (42) revealed that only 10–30% of the marker genes defined in barley displayed a restricted expression in a comparable tissue in *Arabidopsis* (Supplementary Figures S21–S25). Thus, the spatial expression of genes in seeds of the two species shows limited conservation.

A similar comparison was carried out using rice (*Oryza sativa*) RNA-seq expression data in Genevestigator (42) (Supplementary Figures S26a, S26b and Supplementary Table S6). Several genes expressed in the aleurone, endosperm and coleorhiza of barley had enhanced expression in the equivalent tissues of rice, although many did not. Orthology matching between rice and barley is even more complex than barley to *Arabidopsis*, because of the greater number of genes in orthogroups and because different types of datasets are being compared. Consequently, it is not possible to determine if the conservation of expression is greater between barley and rice (both monocots) or between barley and *Arabidopsis* (monocot and dicot), until more extensive and similar datasets become available.

Spatiotemporal analysis of key biological processes during germination of barley grains

To reveal spatial and temporal patterns in the function of expressed genes, functional categories present in at least three time points per tissue or containing at least five genes at any time point were visualised, as well as categories present across the same time point in at least two tissues (Figure 3A). Four major functional groups were identified including DNA/RNA metabolism and translation, seed storage and metabolism, transport and miscellaneous functions (Figure 3A). The majority of genes encoding transcription and translation functions were expressed in the embryo. Specifically, 56–133 genes encoding ribosomal proteins were expressed from 0 HAI to 24 HAI in the embryo tissue, peaking at 24 HAI. A temporal pattern for these was also observed with the expression of 51 and 89 genes encoding ribosomal proteins highly expressed at 24 HAI in the scutellum and endosperm, contrasting with much fewer, if any, observed at other time points for these tissues (Figure 3a). A similar pattern of expression was also observed for the genes encoding transcription factors, elongation factors and heat shock factors, indicating an embryo specific expression pattern, peaking at 24 HAI for many of these genes (Figure 3A). Notably, functions that were associated with translation, ribosomal proteins, elongation factors and heat shock proteins (chaperones), were expressed in the embryo at all time points, compared to other tissues. These spatial gene expression patterns suggest that the ability of germination to proceed without transcription but requiring translation (43,44), is an embryo specific function (Supplementary Table S7 Ribosomal).

Mitochondrial ATP production is critical to support germination. While 88 genes encoding mitochondrial proteins were detected in this study, their expression did not peak in the embryo, and to a lesser extent in other tissues, until 24 HAI (Supplementary Table S7 Mitochondrial). This aligns with phase III of germination (Supplementary Figure S1a) (45). However, the expression of mitochondrial phosphoenolpyruvate carboxylase 1 and phosphoenolpyruvate carboxykinase, along with malate synthase, in only the aleurone tissue at all time points aligns with their role to control the flux of amino acids into gluconeogenesis or protein biosynthesis as documented for oilseeds (46) and barley (47). Notably, most of the energy for germination is derived from glycolysis (47), consistent with 15 mitochondrial transcripts only being observed at 24 HAI. Similar to mitochondrial biogenesis during seed germination in *Arabidopsis* and rice details, in barley, nuclear genes encoding the mitochondrial machinery for transcription and translation are expressed first, enabling the consequent expression of genes encoded in the mitochondrial genome (i.e. *PPR* genes) resumes. This is followed by a later phase in which the nuclear genes encoding proteins for metabolism and the mitochondrial electron transport chain are expressed (48–50).

Distinct functions were also expressed in the endosperm and aleurone. Genes encoding rRNA N-glycosidase and rRNA intron-encoded homing endonucleases were more specifically expressed in the aleurone and endosperm, with 32 of the 93 genes in the genome encoding the latter highly specifically expressed at 24 HAI in the aleurone (Figure 3A). Similarly, genes encoding seed storage and metabolism functions also showed more specific expression in the endosperm and aleurone. Notably, genes encoding late embryogenesis abundant (LEA) proteins also showed temporal specific expression with the highest number of genes expressed at 0 HAI in four of the five tissue types, with the highest number (13 genes) expressed in the 0 HAI coleorhiza tissue (Figure 3A). Dehydrins, which are a type of LEA are known to have important roles associated with phenotypic traits (51) also showed a similar pattern with the eight of the 13 dehydrin encoding genes in the genome expressed at 0 HAI in the coleorhiza (Figure 3A). Based on studies in wheat (52), the expression of prolamin encoding genes such as the low molecular weight glutenin and gamma-gliadin genes were highly specific to the endosperm and here we see this specificity in the aleurone as well (Figure 3A). This pattern was also observed for genes encoding seed metabolism functions, including alpha-amylase, alpha-amylase inhibitor and trypsin inhibitor CME, which is also known to be specific to the endosperm in barley (53). Four genes encoding pathogenesis-related thaumatin like proteins were expressed specifically in the aleurone, with thaumatin like proteins known to have roles in defence, development and seed germination with specific expression

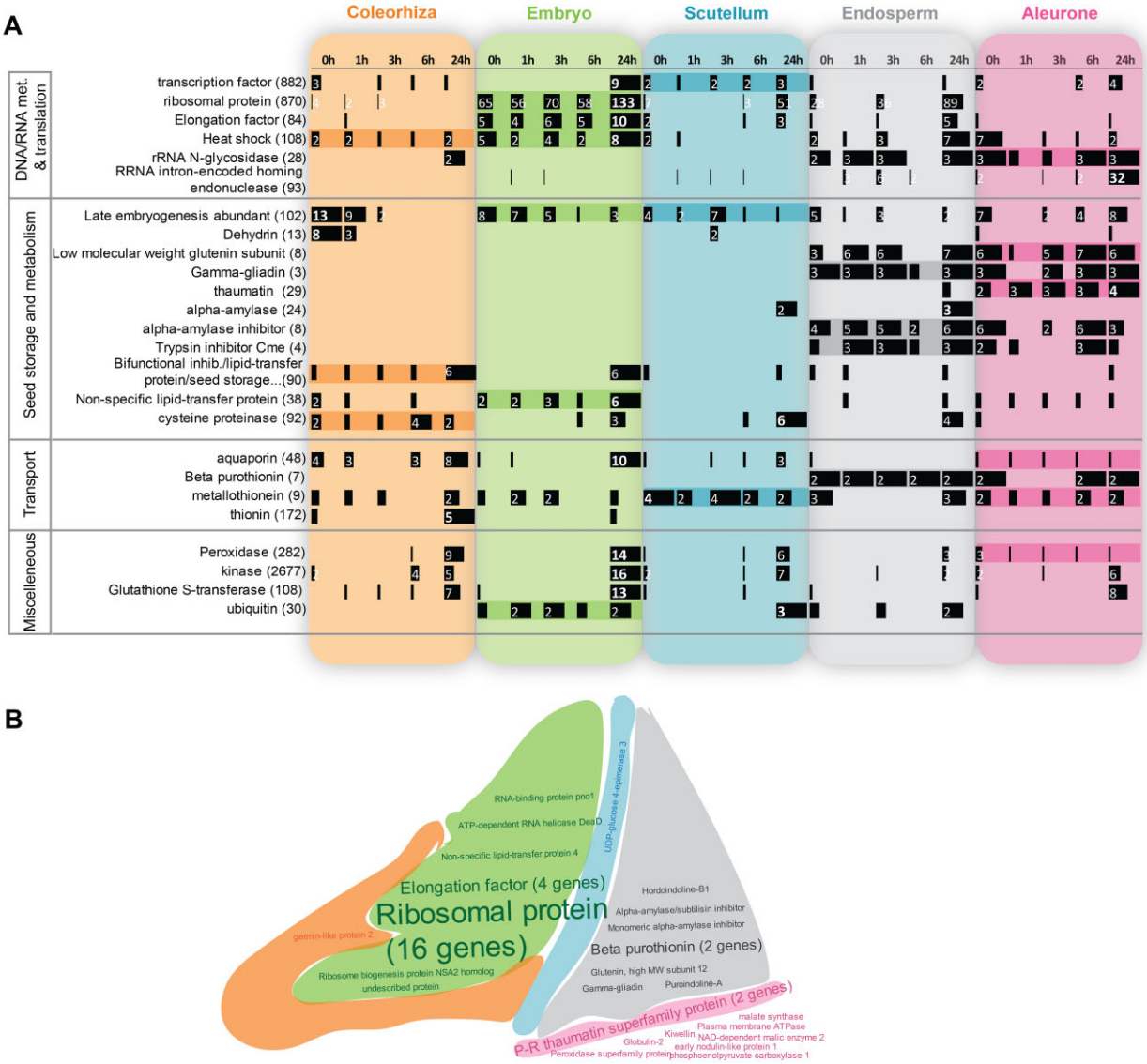

C

Description	Col	Emb	Scu	End	Ale	Locus	Orth - AGI	AGI - description
Metallothionein-like protein 4B	3	3	4	2	5	HORVU1Hr1G052180	AT2G42000	AtMT4a,Type 4 metallothionein (MT) genes. Involved in embryo
						HORVU1Hr1G052180	AT2G23240	AtMT4b,Type 4 metallothionein (MT) genes. Involved in embryo
Histone-lysine N-methyltransferase	4	5	4	2	1	HORVU4Hr1G003060		
undescribed protein	5	5	3	1	1	HORVU5Hr1G002130		
drought-induced 21	4	5	2	3	2	HORVU3Hr1G035470		
60S ribosomal protein L10-2	4	5	2	3	1	HORVU1Hr1G024710	AT1G14320	Ribosomal protein L10, may be involved in translation
						HORVU1Hr1G024710	AT1G26910	Ribosomal protein L16p/L10e family
						HORVU1Hr1G024710	AT1G66580	Ribosomal protein L10 C. Senescence associated gene
Alkaline a-galactosidase seed imbibition protein	4	3	4	1	3	HORVU3Hr1G020780	AT3G57520	ATSIP2, SEED IMBIBITION 2. Raffinose-specific alpha-galactosidase.
Dehydrogenase/reductase SDR family member 4	2	3	3	2	5	HORVU1Hr1G018140	AT1G54870	ChlADR, Choroplast Adehyde Reductase.
						HORVU1Hr1G018140	AT3G05260	NAD(P)-binding Rossmann-fold superfamily protein.
oleosin 1	3	3	3	1	5	HORVU5Hr1G056030	AT5G51210	Oleosin3, involved in seed lipid accumulation.
translationally controlled tumor protein	4	5	4	2	0	HORVU4Hr1G033200	AT3G16640	Translationally controlled tumor protein, TCTP1, likely involved in organ development.

Figure 3. Spatiotemporal analysis of key biological processes during barley germination. (**A**) Tissue specific functional category analysis. The categories identified from wordcloud outputs for the gene lists at each time point and tissue are shown, for those categories identified in at least three time points for a given tissue type or those with >5 genes at a given time point. The numbers of genes expressed at each time point and tissue are represented for each functional category by black bars scaled to the maximum value. The white numbers indicate the genes corresponding to that category at the specific tissue and time point. Bars with no number correspond to 1. Bold white numbers on the bars indicate the category maximum number. The number of genes in the genome for that category is indicated in parentheses. (**B**) Wordcloud categories representing highly tissue specific genes. There were 45 genes identified as having highly tissue specific expression. These were highly expressed in all 5 time points for one tissue, with no expression or specific expression in just one time point in other tissues. (**C**) Most highly expressed genes across all samples. The table shows the genes expressed in 15 or more of the 25 samples making up all time-points and tissues. The number of time points at which a gene is expressed for each tissue is indicated in coloured columns as well as the Arabidopsis orthologue(s) and its description.

observed during germination (54). In contrast to starch metabolism, lipid metabolism functions including bifunctional inhibitor/lipid transfer protein as well as non-specific lipid transfer protein encoding genes showed more specific expression in the coleorhiza and embryo specifically, with the peak number of genes expressed at 24 HAI (Figure 3A).

The initiation of germination in *Arabidopsis* seeds is controlled within the radicle tip by discrete cellular regions that establish a balance between abscisic acid (ABA) and gibberellic acid signalling (55). Initiation of germination in barley seeds and other grasses differs, with the coleorhiza acting as a physical barrier to radicle emergence and thereby promoting dormancy (56,57). Water uptake is one of the earliest events in germination, corresponding with the resumption of core physiological processes (58,59). This is presumably driven by aquaporin transporter proteins (60,61). We observed that some aquaporin-encoding genes were expressed specifically in the coleorhiza and embryo, from 0 HAI and peaking at 24 HAI (Figure 3A, 4, Supplementary Figure S27). Aquaporins are important proteins involved in the movement of water within the seed (60). Initiation of cereal germination also requires weakening of the cell walls in the coleorhiza (56,57). We observed expression of many cell wall modification and degradation-associated genes in the coleorhiza between 0 and 6 HAI, with dynamic changes in expression across this time that likely reflect the complex and rapid events occurring as germination commences (Supplementary Figure S28). Dynamic changes in expression patterns of ABA-related genes were also observed over time in the coleorhiza (Supplementary Figure S29). Whilst the patterns were complex, expression of ABA TFs ABI5 and ABI3, the putative receptor PYR and biosynthetic gene NCDE decreased from 0 HAI onwards.

Temporally specific expression was also observed in the genes encoding thionins (Figure 3A). Notably, of the seven genes encoding beta-purothionins, which are involved in defence (as are thionins) and are known to be expressed in wheat endosperm (62), two genes were expressed in all five time points in the endosperm and three time points in the aleurone, indicating highly specific expression (Figure 3A). It has been shown that beta-purothionins can modify lipid packing and form channels at the bilayer surface to increase water accessibility in the interfacial region (62). Interestingly, four genes encoding metallothionins, out of the nine genes in the genome, showed highly specific expression in the scutellum (Figure 3A), collectively indicating that defence and water transport genes are tightly regulated in a spatio-temporal specific manner during seed germination in barley. Lastly, for the genes encoding peroxidases, kinases and glutathione-s-transferases, it is evidenced that these show a more temporal specific expression pattern with the greatest number of these expressed at 24 HAI and more specifically in the embryo (Figure 3A).

We also identified 45 genes showing exclusive spatial specific expression patterns, defined by expression in all five time points in a particular tissue, with no specific expression or expression in just one time point in other tissues (Figure 3B). In this way, 16 genes encoding ribosomal proteins, four genes encoding elongation factors, other three other genes with RNA binding functions were revealed embryo specific in expression (Figure 3B). Similarly, a gene encoding UDP-glucose 4-epimerase 3 was scutellum specific in expression (Figure 3B), and is orthologous to AtUGE1 and AtUGE3, which are known to be co-regulated with carbohydrate catabolic enzymes and have roles in growth and pollen development (63). Whilst no endosperm specific genes met the above criteria for specificity, eight genes were identified which were expressed at all five time points in the endosperm and at least two time points in the aleurone, shown near the endosperm-aleurone junction (Figure 3B). Notably, two genes encoding beta-purothionins were identified as endosperm-aleurone specific (Figure 3B) and these are known endosperm specific potent antimicrobial proteins in wheat (64). Similarly, gamma-gliadin and glutenin encoding genes were identified as endosperm-aleurone specific here (Figure 3B), and these are known endosperm storage proteins in wheat, with significant roles in affecting flour quality (65). Interestingly, two pathogenesis-related (P-R) thaumatin superfamily protein encoding genes showed aleurone specific expression across all time points (Figure 3B), whilst another two were also aleurone specific but only at 24 HAI (Figure 3A). The *Arabidopsis* orthologue to one of the two aleurone specific genes (*HORVU4Hr1G002650*) is osmotin 34 (AtOSM34), which has been shown to function as a positive regulator of ABA responses is under post-translational control (66), thus further investigation into the function of these in barley germination could reveal insight into whether this regulatory role is conserved.

Lastly, to identify genes that were not specific to a given tissue, genes that were expressed in at least 15 of the 25 samples making up the five time-points in the five tissues were examined, revealing nine genes (Figure 3C). Six of these had 10 *Arabidopsis* orthologues (OMA browser) (26), all of which were expressed across the developmental tissues (BAR). Apart from *At3G57520* and *At3G16640*, which showed moderately high expression during germination, the other eight genes showed the highest expression in dry seeds and/or during seed germination. For example, all three *Arabidopsis* genes that were orthologous to the barley 60S ribosomal protein L10-2 (*HORVU1Hr1G024710*) were co-expressed showing maximum expression in the germinating seed specifically. Similarly, both *Arabidopsis* genes orthologous to barley metallothionein-like protein 4B (*HORVU1Hr1G052180*) and both *Arabidopsis* genes orthologous to dehydrogenase/reductase SDR family member 4 (*HORVU1Hr1G018140*) showed maximal expression in the dry seed, just prior to germination. Notably, reducing expression of both *AtMT4a* and *AtMT4b* resulted in reduced seed weight and affected post-germinative early seedling growth, with over-expression resulting in the opposite effects (67). The same study also revealed these to have a role in zinc accumulation in seeds, thus this gene in barley could represent a conserved orthologue, possibly having a similar role. Likewise, the other *Arabidopsis* genes that were orthologous to other genes in barley (Figure 3C) have been shown to have roles in seed lipid accumulation, embryo development and organ development (Figure 3C), thus the conserved expression revealed here could suggest these genes may have similar functional roles in seeds and development in barley. Interestingly, the three genes encoding a histone-lysine

N-methyltransferase (*HORVU4Hr1G003060*), an undescribed protein (*HORVU5Hr1G002130*) and drought-induced 21 (*HORVU3Hr1G035470*) did not have significant orthologues in *Arabidopsis*. Considering their expression in all five tissues and at multiple time points for most tissues suggest these could be excellent targets to examine for functional roles in seed germination in barley.

Aquaporin gene family members have distinct spatiotemporal expression patterns

We dissected further the spatial expression of genes by examining in greater resolution the expression of some gene families associated with the functions outlined above. In addition to water, transport of ions, solutes and other elements is essential for successful germination and occurs during imbibition in the earliest phase of germination (45,68). We assembled a list of genes encoding proteins involved in transport processes, focusing on aquaporins (Figure 4A, full list in Supplementary Figure S27). Aquaporins are best known for their ability to facilitate water flow, but also transport various ions, solutes and CO_2 (69). They are located in the plasma membrane (plasma membrane intrinsic proteins, PIPs) or the tonoplast (tonoplast intrinsic proteins, TIPs). Some rice aquaporins, OsPIP1;1 and OsPIP2;1, promote rice germination (70) and root growth (71). Consequently, the expression patterns of several TIPs and PIPs were assessed (Figure 4A). Interestingly, at 24 HAI, we found highly expressed isoforms in the mesocotyl, scutellum and coleorhiza (Figure 4B), illustrating that expression of aquaporin family genes is highly spatially distributed and organised during germination. The gene *HORVU4Hr1G079230* encodes a tonoplast intrinsic protein 1;1 (TIP1;1) that is the most abundantly expressed isoform of the TIP family (72), which was also confirmed by our data. TIP1;1 is a housekeeping aquaporin and establishes a basal level of tonoplast hydraulic conductance (73,74). In the spatial transcriptomic data, it was expressed mainly in the coleorhiza at early timepoints (0–6 HAI), then expression strongly increased at 24 HAI in coleorhiza and in the radicle and mesocotyl of the embryo (Figure 4C, top). Another aquaporin gene, *HORVU1Hr1G043890,* encodes tonoplast intrinsic protein 3;1 (HvTIP3;1) which accumulates in the aleurone and outer layers of the barley seed (75). We found this gene to be highly expressed in the embryo tissues at 0 and 1 HAI, followed by expression in the scutellum and aleurone layer at 3 and 6 HAI and in some areas of the aleurone/subaleurone layers at 24 HAI (Figure 4C, bottom). These results illustrate the different spatiotemporal expression patterns of gene family members and how specific aquaporins regulate water transport in distinct tissues during seed germination.

Activation of mitochondria, respiration and ATP synthesis are upregulated in the early stages (phase II) of germination (Supplementary Figure S1a). This indicates that ATPases and organellar transporters were another important subset of transporter genes (Supplementary Figure S30a). Expression of the gene *HORVU6Hr1G070780* was strongly spatially localized. This gene encodes an adenine nucleotide translocator that carries ADP/ATP across the mitochondrial membrane, providing the seed with the required energy to ensure growth (76). Our spatial images showed increasing expression of this translocator in the coleorhiza, embryo and scutellum during early imbibition (0–6 HAI) followed by a high expression across all tissues but with a focus on the transition zone between scutellum and endosperm at 24 HAI (Supplementary Figure S30b). The gene *HORVU2HR1G111640* encodes a cation-transporting H(+)-ATPase. This ATPase pumps protons out of the cell, generating a proton gradient which drives the active transport of nutrients by proton symport (77). This process has been studied in maize showing the apoplast acidification is used to promote secondary transport of nutrients and cell elongation (78). We detected expression of this proton pump in the aleurone layer at 3 and 6 HAI and, by 24 HAI, expression had spread to the endosperm and strongly in the vicinity of the scutellum (Supplementary Figure S30b). This result supports the idea that the nutrients stored in the starchy endosperm are mobilised after imbibition, absorbed by the scutellum and later transported to support growth of the embryonic axis.

Mobilisation of reserves and starch metabolism

Barley seeds store their energy reserves in the form of starch in the endosperm, which is then degraded during germination to fuel embryo growth, as is common amongst many cereals (79). As mentioned above, H(+)-ATPase activity acidifies the endosperm, which favours the solubilisation of the starch and the stability of alpha-amylase (Supplementary Figure S30b) (78). The expression of starch metabolic genes was visualised to better understand their spatiotemporal expression (Figure 5A). Whilst starch synthesis genes were predominantly expressed in the aleurone at 0 HAI, the starch degradation enzymes were highly and diversely expressed across germination (38,80). Starch catabolism requires the combined action of alpha- and beta-amylases to breakdown starch into smaller oligosaccharides and the alpha-glucosidases, and convert it into glucose (81). The spatiotemporal expression of the genes involved in this pathway was clearly depicted by our ST data (Figure 5B). Beta-amylases (BAM) hydrolyse starch during the first 24 HAI, as exemplified by BAM1 (*HORVU4Hr1G089510*) which was highly expressed across germination (0–24 HAI), predominantly in aleurone and the distal endosperm (furthest from embryo). The same pattern was observed for some protease inhibitors, including most of the alpha-amylase inhibitor (AAI) gene family (i.e. AAI4, *HORVU7Hr1G035020*) and the gene *HORVU2Hr1G090750* gene, which is a kunitz-type (KUN1.1) protease proposed to have a role in pathogen protection and to limit the degradation of starch (82). The gene *HORVU7Hr1G106540* is an alpha-glucosidase (AGL) 1 involved in starch degradation and known to be highly expressed in the germinating barley grain (81). We observed that AGL1 expression was upregulated at 6 HAI in the scutellum, then increases along the scutellum and in the embryo-endosperm junction at 24 HAI. Alpha-amylases expression (alpha-Amylase1_1c, Amy1_1a and Amy2_1) was also observed in the embryo-endosperm junction at 24 HAI (Figure 5C). Previous studies in rice and barley have shown that alpha-amylases are critical for

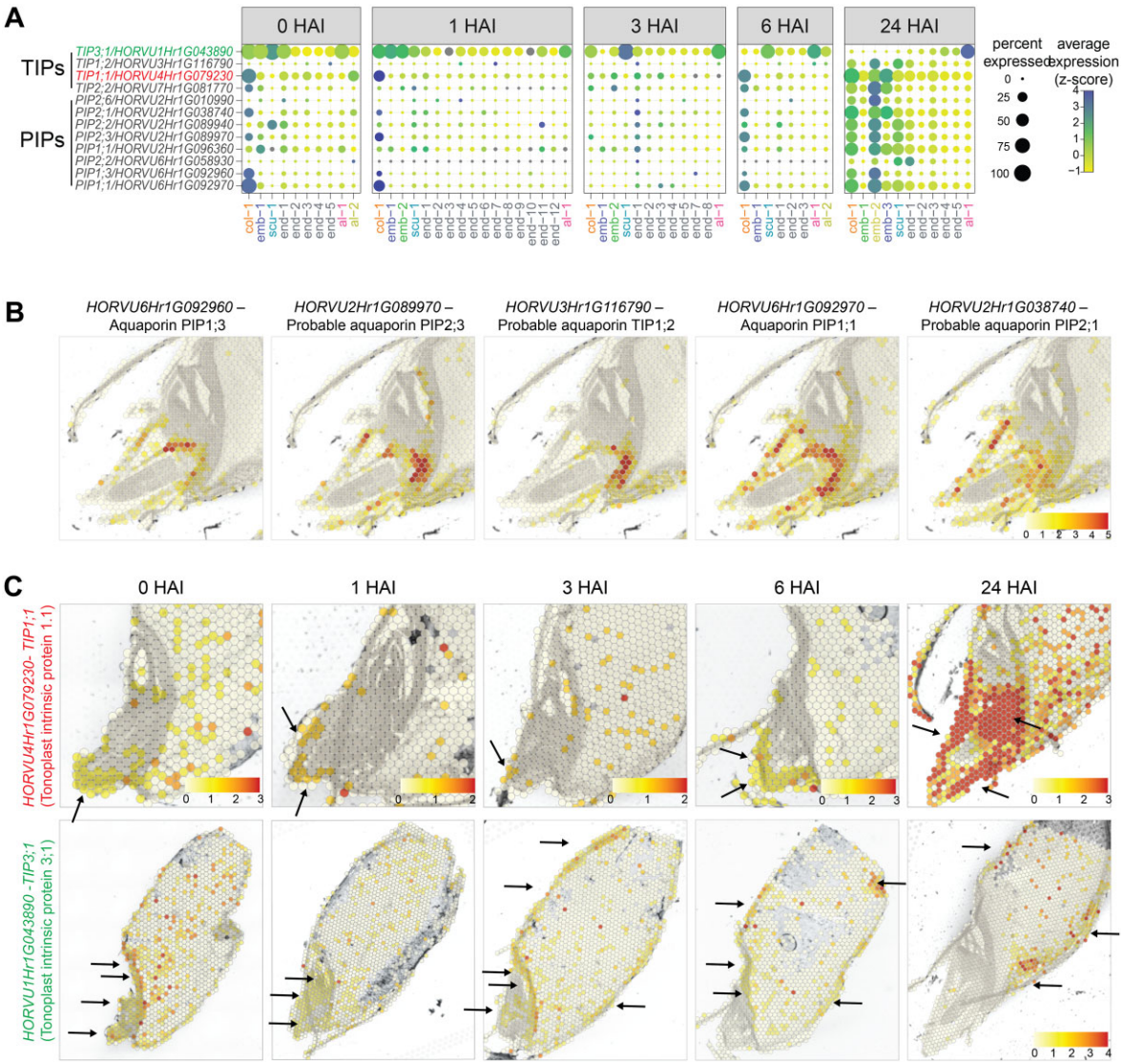

Figure 4. Spatio-temporal expression of aquaporin genes during barley germination. (**A**) Bubble plots showing the spatially resolved expression of aquaporin gene family members (plasma membrane intrinsic proteins, PIPs; tonoplast intrinsic proteins, TIPs) across the experimental time-course. Circle size indicates the percentage of expression and colour indicates average expression after *z*-scoring. The x-axis represents individual clusters identified across tissues. For genes highlighted in green and red expression patterns are also shown in c). (**B**) Highly expressed aquaporin family genes and their specific locations at 24 HAI. (**C**), Time course expression of TIP genes: *HORVU4Hr1G079230* (TIP1;1) gene at the top panel and *HORVU1Hr1G043890* gene (TIP3;1) at the bottom panel. Colour scales represent the normalised counts with the same cut-off in each row or with cut-offs individually specified on the image. Black arrows indicate areas of expression. col: coleorhiza, emb: embryo, scu: scutellum, ale: aleurone, end: endosperm.

seed germination (38,83). From our spatiotemporal data of germination, both alpha- and beta-amylases appeared to participate in early sugar breakdown steps as previously reported in wheat (84), and it was clear they execute their functions in different locations of the germinating grain. Altogether, these results indicate the tight and localised control of starch degradation during early germination.

Cell division during barley germination

The cell-cycle arrests at the end of seed development, with barley embryo cells primarily arresting in the G1 and G2 phases (85). Reactivation of the cell-cycle must occur during germination for embryo growth to proceed. Previous expression analysis detected transcription of cell cycle-related genes only once the radicle had started to protrude, which is at the end of germination (86,87). Consistent with this, we found that few cell-cycle related genes were expressed in our spatial analyses during the early phases of time course, 0–6 HAI and that a subset of these genes were then expressed at the 24 HAI mark (Supplementary Figure S31).

Expression dynamics of cell wall metabolism genes

Transcription of genes involved in cell wall metabolism are up-regulated during the early stages of seed germination (88) (Supplementary Figure S28). Cell wall degradation, modification and precursor synthesis are essential processes in weakening of the tissues, e.g during radicle expansion. We detected spatially distinct and dynamic expression

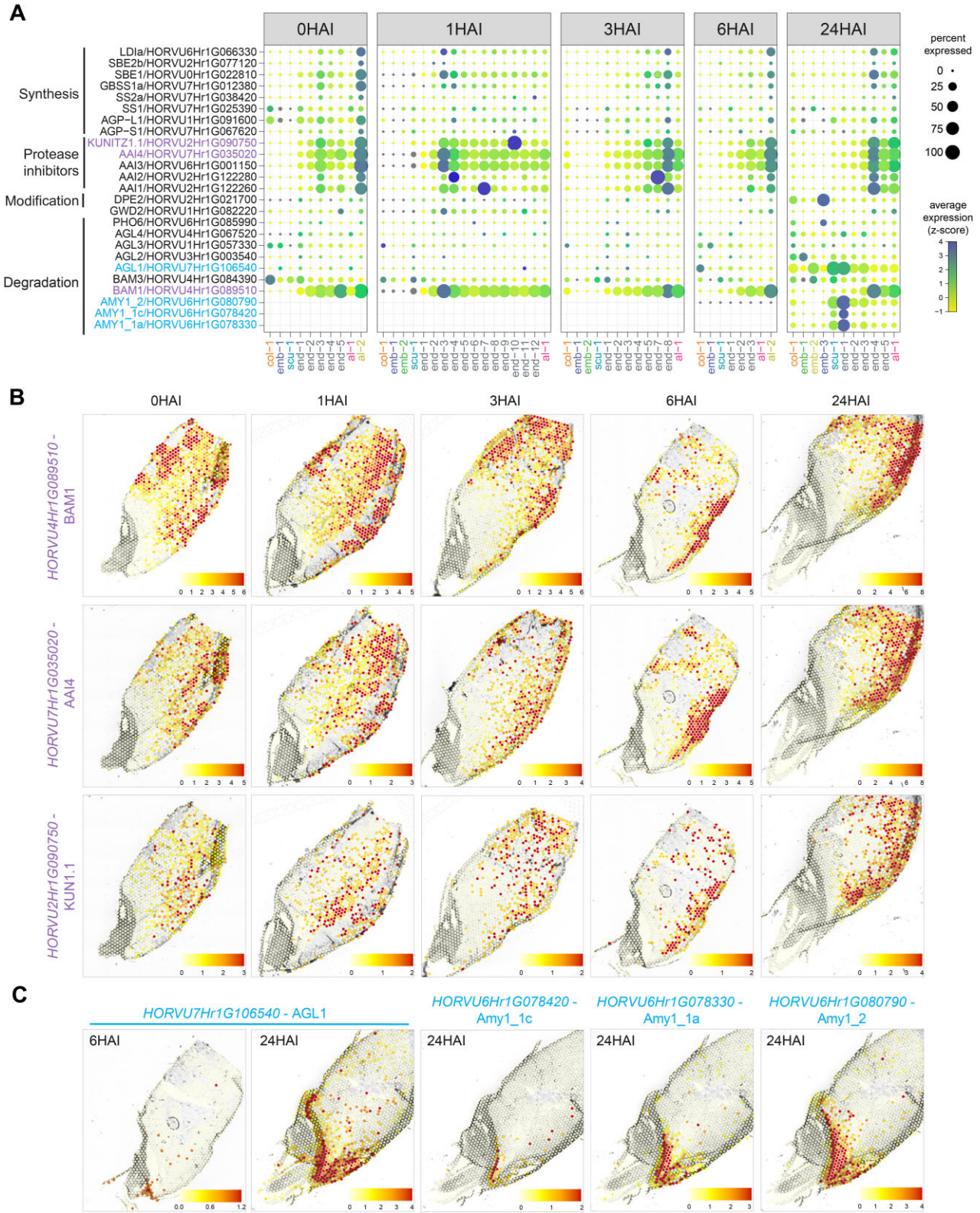

Figure 5. Spatio-temporal expression of carbohydrate-related genes during barley germination. (**A**) Bubble plots showing the spatially resolved expression of starch-related genes across the experimental time-course. Circle size indicates the percentage of expression and colour indicates average expression after *z*-scoring. The x-axis represents individual clusters identified across tissues. For genes highlighted in purple and blue, expression patterns are also shown in B and C. (**B**) Time-course expression of *HORVU4Hr1G089510* gene (beta-amylase/BAM1) at the top panel, *HORVU7Hr1G035020* gene (alpha-amylase inhibitor/AAI4) in the middle panel and *HORVU2Hr1G090750* gene (Kunitz-type protease inhibitor/KUN1.1) at the bottom panel. (**C**) Spatial expression of *HORVU7Hr1G106540* gene (alpha-glucosidase/AGL1) on the left panels and alpha-amylase family genes (Amy1_1c, Amy1_1a and Amy1_2) on the right panels. Colour scales represent the normalised counts with the same cut-off in each row or with cut-offs individually specified on the image. Black arrows indicate areas of expression. col: coleorhiza, emb: embryo, scu: scutellum, ale: aleurone, end: endosperm.

of cell wall-related genes across barley grain germination. For example, *HORVU3Hr1G073780*, encoding a type of cellulose synthase, was expressed at a relatively low level up until 6 HAI, but increased at 24 HAI (Supplementary Figure S32a). It further displayed a very particular spatial pattern in the radicle, possibly the epidermis and cortex, suggesting this gene might be involved in new cell wall formation. Expansins were originally identified because of their ability to induce cell wall extension and are key regulators of cell growth (89). We found that *ALPHA EXPANSIN 2* (*HORVU3HR1g081180*) was highly expressed in late germination (6 and 24 HAI) around the expansion zone of the radicle (Supplementary Figure S32b), implicating it in radicle protrusion for germination. Another cell wall-related gene, *HORVU5HR1g080860*, encodes a UDP-glucose epimerase (*HvUGE*) which participates in sugar precursor synthesis for cell wall biogenesis. Despite being identified in barley developing seed, leaf tips and mature roots (90), our spatial study located *HvUGE* in the scutellum at all time points of germination (Supplementary Figure S32c), which suggests this epimerase participates in cell wall polysaccharide synthesis during several barley developmental stages.

Transcription factors involved in the spatiotemporal gene regulatory landscape

We sought insight into the gene regulatory landscape in barley by examining the expression of genes encoding transcription factors (Supplementary Figure S33). One of the strongest expressed genes encoding a transcription factor was *HORVU1Hr1G086580*, a bZIP type transcription factor that responds to karrikin. Karrikins are small organic compounds known to be promoters of germination (91). The spatial expression of *HORVU1Hr1G086580* is highest in early germination (0–3 HAI) in the scutellum and the adjacent endosperm area and then declines during germination (Figure 6B i). An *Arabidopsis* ortholog, delay of germination 1-like 4 (DOGL4/*AT4G18650*), is a maternally expressed imprinted gene found in the endosperm of dry seeds and was described as a negative regulator of seed dormancy (92). The *HORVU4Hr1G009730* gene encodes the barley knox 3 (BKN3) transcription factor that plays a pivotal role in shoot apical meristem (SAM) formation and maintenance as well as some morphogenetic processes during plant development (93). We detected no expression of *BKN3* during early phases of germination (0–6HAI), but a very distinctive and localised expression at 24 HAI in the SAM (Figure 6B ii). The *HORVU2Hr1G104040* gene encodes a novel myc-related bHLH transcription factor and its ortholog in *Arabidopsis, Phytochrome-interacting factor 1* (*PIF1*), mediates light-regulated control of seed germination (94,95). Our analysis showed that it is not expressed during early stages of germination (0–6 HAI) but expressed at 24 HAI in the scutellum (Figure 6B, iii). Another transcription factor, *HORVU7Hr1G026940*, encodes a DREB subfamily A-5 of ERF/AP2 transcription factor. DREBs are dehydration response element binding factors and one of the main groups of transcription factors that regulate expression of abiotic stress-inducible genes (96). Spatial transcriptomics showed the expression of this transcription factor was restricted to the scutellum and endosperm during the early time points of germination (0–3 HAI) but it increased and moved to the aleurone layer at 6 HAI and 24 HAI (Figure 6B, iv).

It is clear from the above examples for critical processes in germination that considerable variation in transcript abundance occurs with tissues (i.e. clusters) that has previously gone undetected.

Non-biased discovery approaches define spatiotemporal domains during seed germination of barley

Expression of genes is not necessarily uniform across all cells within a tissue or cluster. Non-uniform expression within tissues reflects spatial organisation of function within that tissue. We assessed the ability of spatial transcriptomics to identify genes that had discrete patterns of spatial expression within tissues. To do so, we focussed on the embryo tissues across all time points and applied Moran's I spatial autocorrelation statistics to all expressed genes. This metric defines the correlation of gene expression of a local spot with its neighbouring spots and thus is a measure for non-random spatial patterns (see method for details) (97). Moran's I varies from –1 to 1, and a positive value indicates that cells with similar gene expression patterns are clustered together in a coherent domain. A value close to zero designates random spatial distribution of similar gene expression patterns, whilst a negative value shows that cells with similar gene expression patterns are spatially separated from each other. We considered genes that had a Moran's $I > 0.25$, an adjusted P value < 0.01, expression in >5% of spots in a section, and meeting those thresholds in at least two sections for a time point, as having coherent expression domains; these are subsequently referred to as spatially variable genes (SVGs) (98). The lowest number of SVGs was detected at 3 HAI and the highest number at 24 HAI (Figure 7A, Supplementary Table S8). Among those SVGs, there were 204, 147, 68, 201 and 1098 SVGs consistently detected in all four sections for 0 HAI, 1 HAI, 3 HAI, 6 HAI and 24 HAI, respectively (Supplementary Figure S34, Supplementary Table S8).

Many SVGs also had temporally specific expression; 1812 SVGs were specific to one time point whilst 755 were spatially variable in more than one time point (Figure 7bB). Combined spatiotemporal expression patterns of SVGs were diverse. For example, a histone deacetylase 2B (HD2B, Figure 7C, i) with a Moran's $I = 0.64$ at 24 HAI, was enriched at the active growth centres including the radicle and shoot meristem in the embryo. HD2B histone deacetylase is associated with seed dormancy in *Arabidopsis* (99). Two components of the histone deacetylation complex positively regulate seed dormancy while inhibiting seed germination by integrating ABA, ethylene and auxin signalling pathways (100,101). *HORVU4Hr1G003340*, an ortholog of *Arabidopsis* bHLH25, is a transcription factor enriched in the radicle at 24 HAI (Moran's $I = 0.63$, Figure 7C, ii). Overexpression of *Arabidopsis* bHLH25 results in increased lateral root numbers (102). *HORVU7Hr1G042390* encodes a homolog of the GAST1 protein homolog 4 (GASA4) protein, which is a regulator of gibberellic acid-dependent seed germination and expressed in the shoot apex and embryo

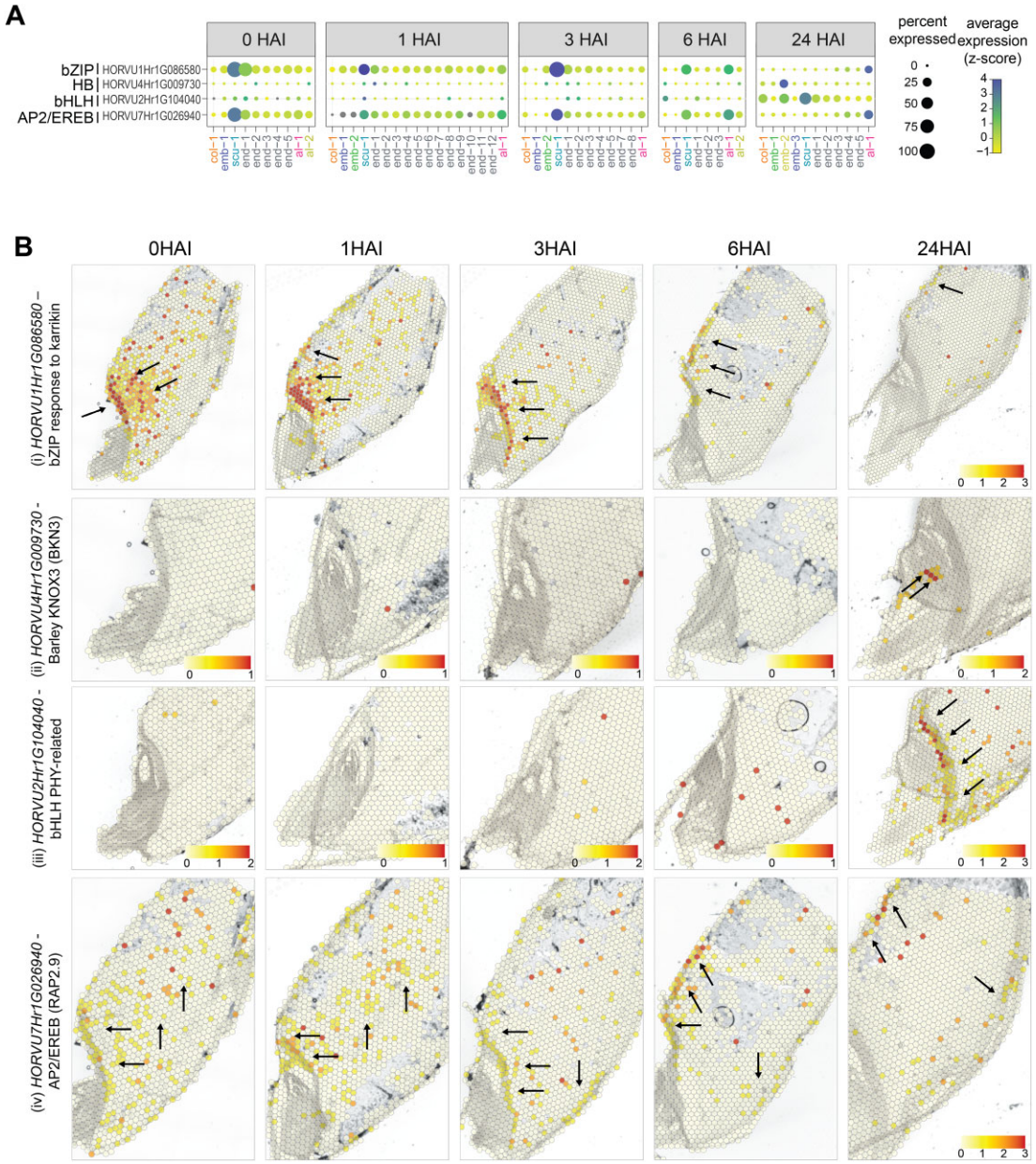

Figure 6. Spatio-temporal expression of transcription factors during barley germination. (**A**) Bubble plot showing the spatially resolved expression of several transcription factor encoding genes. Circle size indicates the percentage of expression and colour indicates average expression after *z*-scoring. The x-axis represents individual clusters identified across tissues. (**B**) Spatial expression of transcription factor genes, (i) Karrikin-responsive bZIP (ii) *BARLEY KNOX3* (*BKN3*), (iii) bHLH PHY-related and (iv) AP2/EREB RAP2.9. Colour scales represent the normalised counts with the same cut-off in each row or with cut-offs individually specified on the image. Black arrows indicate areas of expression. Col: coleorhiza, emb: embryo, scu: scutellum, ale: aleurone, end: endosperm.

in *Arabidopsis* (103,104). Its expression was focussed on the coleoptile with Moran's I = 0.6 (Figure 7C, iii), consistent with the important role of GA in seed germination (105). Moreover, the previously identified coleoptile-specific gene, *HORVU4Hr1G022780*, encoding a non-specific lipid-transfer protein 4, was also identified as an SVG (Figure 7C, iv).

Groups of SVGs may be expressed within similar spatial patterns because they have related or associated functions in the underlying cells. To examine this potential spatial co-expression we performed a high dimensional co-expression network analysis with the 1889 significant SVGs from 24 HAI sample using hdWGCNA (28). We determined seven co-expression modules and visualized their spatial expression patterns using eigengenes, which represent the common expression pattern of all genes within a module (Figure 8A, Supplementary Table S9). Gene functions within modules were assessed using gene ontology (GO) enrichment analysis (Figure 8B). Genes in the green module were highly expressed in the apex of radicle and were enriched for functions in glutathione (GSH) metabolic processes and sulfur compound metabolic processes. GSH is critical for

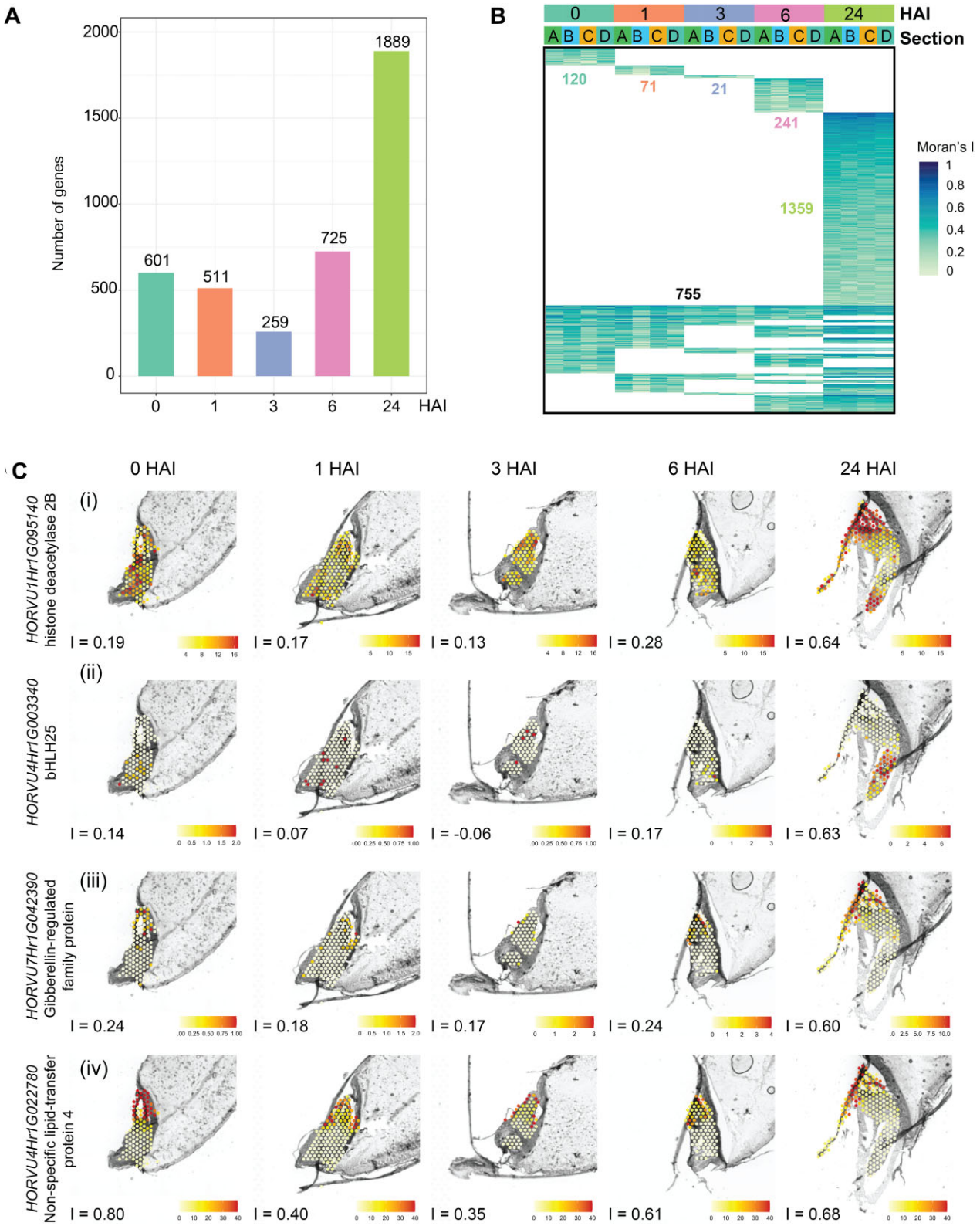

Figure 7. Spatial autocorrelation defines domains in the embryo of the germinating barley grain. (**A**) Number of SVGs showing significant spatial coherence for each time point. For each section, Moran's I was calculated for embryo-expressed genes, and genes with Moran's $I > 0.25$, adjusted $P < 0.01$ and expressed percentage in embryo spots > 5% were considered having significant spatial coherence within a domain of the embryo. For each time point, SVGs showing significant spatial heterogeneity in at least two sections were plotted. (**B**) Heatmap showing the Moran's I of 2567 SVGs showing significant spatial coherence. The coloured text and black text indicate the number of time point-specific and time point-common genes, respectively. (**C**) Examples of SVGs increasing spatial coherence. Colour scales represent normalised counts. *I*, Moran's *I* value.

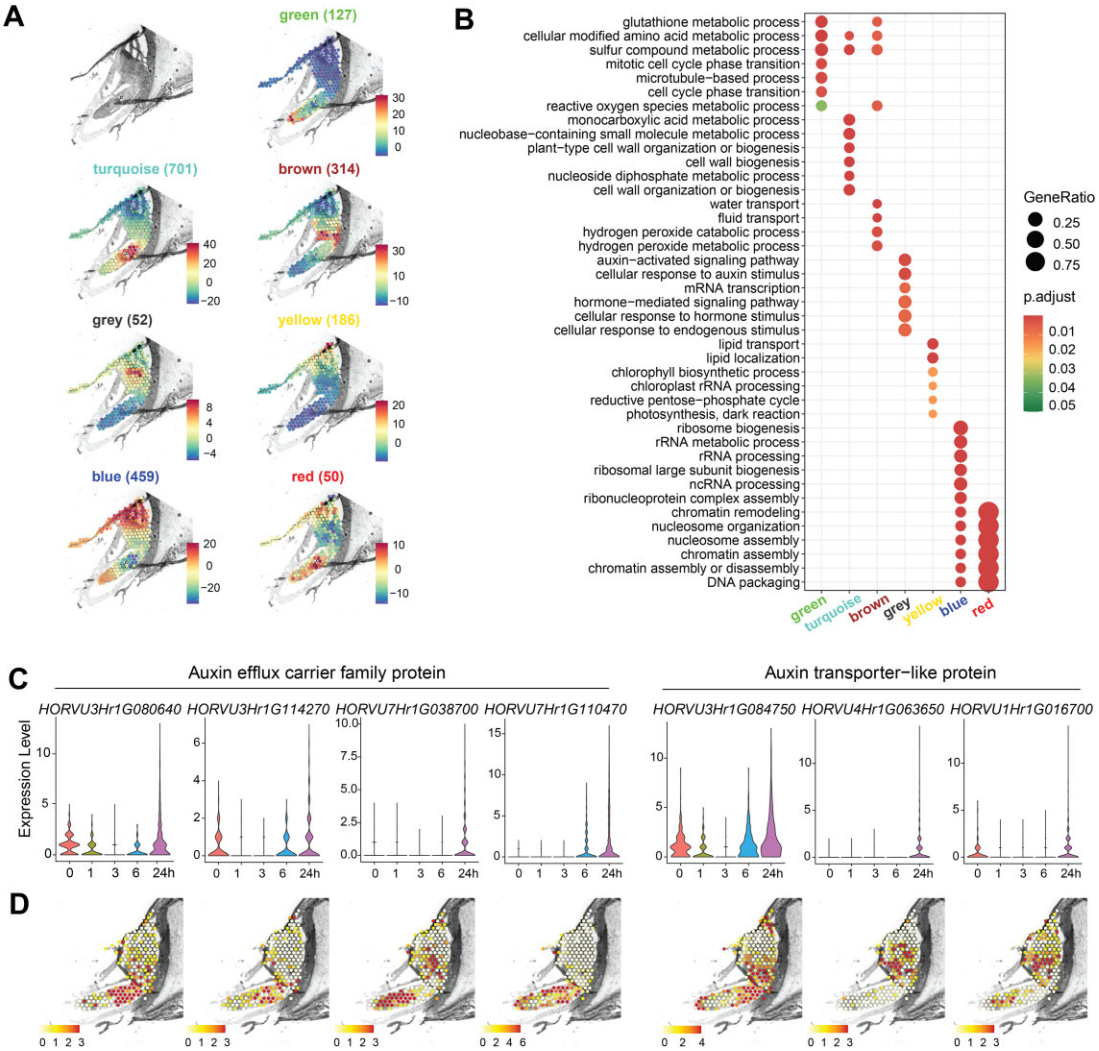

Figure 8. Co-expression of spatially variable genes in the embryo of 24 HAI germinating barley grain. (**A**) Module eigengenes, a proxy for expression of genes within each module, of seven co-expressed modules. The top left panel show the bright field microscopic image, the other panels show the overlayed expression data for spots. SVGs showing spatial coherence in embryo of 24h germinating barley grain were grouped into co-expression modules using hdWGCNA (28). Gene number in each module is given in the brackets. (**B**) Gene Ontology enrichment of the co-expression modules. The top six enriched biological process terms for each module are shown. GeneRatio: number of genes annotated with a GO term in a cluster divided by the total number of genes annotated with this GO term. p.adjust: adjusted *P* value using Benjamini & Hochberg method. (**C**) Expression of auxin efflux carrier and transport genes showing spatial coherence at 24 HAI. Normalised counts were used to indicate expression level. (**D**) Spatial expression of auxin efflux carrier and transport genes showing spatial coherence, colour scales represent normalised counts.

(embryonic) root development in *Arabidopsis*, partly via modulation of auxin transport and signalling (106–108). The turquoise module was expressed most highly at the base of the radicle and enriched for cell wall biogenesis and organization functions, which are important developmental processes for radicle emergence (109–111). The brown module was expressed most highly in the mesocotyl and genes within this module were associated with water and fluid transport, which corresponds to the presence of the vascular tissues in this region. The yellow module was expressed most highly in the coleoptile and consisted of genes enriched in photosynthesis and chlorophyll biosynthetic processes. This corresponds to the role of the coleoptile as the first photosynthetically active tissue during transition from heterotrophic to autotrophic growth. Expression of the blue and red modules was highest in the embryo root and shoot, with expression of the blue module highest in the embryo leaves whilst the difference between the embryonic leaf and root was less notable in red module. Both modules were enriched for chromatin and nucleosome assembly, with the blue module is also enriched for ribosome biogenesis. This is consistent with the known presence of rapidly dividing cells in these meristematic regions. The grey module was highly expressed in the shoot apical meristem and consisted of genes involved in auxin signalling. In summary, this analysis was able to correlate functional relationships of genes and their spatial distribution on a sub-tissue level.

Auxin has a critical role in embryo development and growth (112,113). An in-depth evaluation of the SVGs list revealed 24 auxin-related genes showing spatially

variable expression in at least one time point, with 18 of them found at 24 HAI (Supplementary Table S8). From these 18 auxin-related genes, we further focused on seven genes which belong to auxin efflux carriers and transporter − like families (Figure 8C). An auxin efflux carrier family protein (*HORVU7Hr1G038700*) and one auxin transporter-like protein (*HORVU4Hr1G063650*) were mainly expressed at 24 HAI while the other five genes were dominantly expressed at more than two time points (Figure 8C). Interestingly, the four auxin efflux carrier genes were mainly expressed in the embryo root and enriched towards the base of the radicle (*HORVU3Hr1G080640*, *HORVU3Hr1G114270*), the inner embryo apex (*HORVU7Hr1G038700*) and epidermis (*HORVU7Hr1G110470*) (Figure 8D). The three members of auxin transporter—like proteins also displayed an obvious spatial-dependent expression pattern (Figure 8D). Auxin transporter—like protein 1 was enriched in the mesocotyl as well as the root tip. Auxin transporter—like protein 2 and 3 are both enriched in the embryo SAM with auxin transporter—like protein 3 also showed high expression in the inner layers of the embryo radicle. The complementary expression of those auxin-related genes suggests the transport and accumulation of auxin in the barley embryo is controlled by a spatially complex distribution of auxin transporters, similar to what is known in rice (114) and the well-define role of auxin for the formation of the embryonic apical–basal axis established in *Arabidopsis* (115).

DISCUSSION

Here, we have presented a spatially resolved transcriptomic analysis of germinating barley grain at a resolution of 55 μm over 24 HAI. The accuracy of the spatial determination of expression was confirmed using RNA *in situ* hybridisation. The quantitative nature of the approach shows reasonable correlation with bulk RNA-seq. As different cells will be expressing genes at different levels depending on the cellular landscape (35), such variation is lost in bulk-sequencing, but retained in spatial transcriptomics. The number of genes detected and that changed in expression in our study was also comparable to bulk sequencing. We developed a web application to allow users to visualize and explore our datasets. The web application gives access to: (i) the spatial distribution of clusters in four sections for each time point; ii) expression of genes of interest in a spatial way as well as UMAP and Violin plot; (iii) expression of embryo SVGs; (iv) marker gene list of each time point and Moran's I value for embryo SVGs. The web application can be accessed at https://spatial.latrobe.edu.au.

In our experiments, we observed consistently isolated individual spots of expression for some genes on single sections. The biological interpretation of such isolated expression is unclear; does it represent transcriptional 'noise' that has been proposed to occur (116), or does it represent an artifact? A larger number of replicates will help interpret such signals, and these larger datasets will additionally drive the development of bioinformatic approaches to allow individual cell expression to be visualised and placed in context of the transcriptional landscape of the tissue as a whole. As an advantage for plant biology, the spatial transcriptomic approach works well with fresh frozen tissue. The ability to obtain cell sections from a large variety of plant tissues even with limited amounts means that profiling of cells that have been previously lost either in bulk or protoplast approaches because of their limited numbers will be avoided. A cost limitation currently of this technology is to develop a 3D cell expression atlas of the target tissue. This would require at least tens of sections at each time point. With different commercial technologies emerging in this area and uptake cost should come down in the future (117), but large scientific consortia like the Plant Cell Atlas (https://www.plantcellatlas.org) and STOC (Spatio-Temporal Omics Consortium- https://www.sto-consortium.org/news_events.html) will be valuable in providing access to individuals to larger funded studies.

From our data the spatial heterogeneity in expression of gene family members and their gradients of expression over time were apparent. The analyses revealed that significant enrichment of different processes occurs in specific locations, i.e. translation in the embryo (Figure 3), auxin signalling pathways in the coleorhiza (Figure 8). It is well established that translation, not transcription, is essential for germination to commence. This study shows that this is confined to the embryo, and that 45 genes encoding proteins associated with translation are embryo specific. A variety of genes in other tissues that are associated with grain or processing quality, gamma-gliadin, can also now be located to specific areas and promoters associated with this expression defined. Auxin has emerged as a key player in regular pattern for the formation of lateral roots with oscillations in auxin defining the lateral root pattern (118–120). An auxin maximum precedes lateral root formation which depends on auxin transport. Furthermore, the repression of lateral roots in response to loss of contact with water is regulated by movement of ABA from the phloem (121). Here, we show that genes encoding auxin transporters already show spatially distinct patterns at the time the radicle emerges from the seed coat. Knowing what auxin transporter(s) (and other hormone transporters) are expressed where and how they respond to environmental changes will allow breeding strategies to target these processes more efficiently. Previously it has been shown that auxin represses aquaporin expression to allow lateral root emergence. The spatial and temporal expression patterns determined here can identify the molecular components involved in this process (122) and provide approaches to alter these responses for agricultural purposes.

Comparison of marker genes defined using spatial transcriptomics in this study to orthologs in *Arabidopsis* and rice revealed that while some had similar a same expression pattern on a tissue basis, the majority did not. This is similar to studies using scRNA-seq showing the expression of some genes in meristems (root or shoot apical meristem) were conserved and, in general, patterns are conserved across species when similar functions and structures are required (9). Approximately 65% of genes in plant genomes are duplicates and most crops are polyploid, consequently for many important agronomic traits such as seed size and disease resistance the spatial expression pattern of genes arising from subfunctionalisation and subneofunctionali-

sation is an important mechanism for retaining duplicates (123). Thus, determination of the precise sub-tissue expression pattern of genes is key to using molecular approaches for plant improvement in the future.

It is essential that crop varieties that respond to environmental changes are developed to produce the food for a growing world population. While the cessation of growth under environmental limitations has been traditionally viewed as a resource allocation problem, i.e. resources are used for pathogen defence not growth, detailed molecular studies have revealed that growth limitation is due to antagonistic transcriptional pathways (124). For example, mutation in *PHYTOCHROME B* rescues the growth retardation of jasmonate mutants that have a constitutively active defence response, but this depends on the levels of the defence response and tryptophan biosynthesis (125). It has also been shown that different stresses can be mediated via different tissue types (126). Thus, the understanding of where genes are expressed and how they respond to environmental conditions is vital to future strategies to breed plants that can respond to the environment and maintain growth (127). The concept of specialised plastids is proposed for sensing and responding to stress in a tissue specific manner (128). Spatial transcriptomics provides the high throughput technique to allow these emerging concepts to be developed and further our knowledge of how plants respond to the environment from a cellular to whole plant level.

While we could dissect many important processes of seed germination, some aspects were not completely covered by our approach. For example, we only partially covered hormonal pathways, with GA synthesis occurs in scutellum and aleurone (129,130) and ABA synthesis in endosperm/aleurone and embryo (130). This may be due in part to depth of coverage, but we also took a conservative approach in defining presence of transcripts. the thickness of the sections (eight μm) restricts the coverage of the seed, and thus more sections, longitudinal and transverse will be required. These limitations, in addition to the currently prohibitive costs, will be overcome with the diverse range of technologies for spatial transcriptomics (131,132) and/or a combination of spatial and scRNA-seq (22).

DATA AVAILABILITY

The accession number for the raw sequencing data and Space Ranger processed data reported in this paper is Gene Expression Omnibus (GEO): GSE218970 (https://www.ncbi.nlm.nih.gov/geo/). Any additional information required to reanalyse the data reported in this paper is available upon request.

The interactive web browser can be explored at https://spatial.latrobe.edu.au/.

SUPPLEMENTARY DATA

Supplementary Data are available at NAR Online.

ACKNOWLEDGEMENTS

We thank Associate Professor Matthew Tucker for kindly providing the barley grains used in this work. We thank Dr Jacqueline Orian and her laboratory for their guidance setting up the cryosectioning.

Author contributions: J.W., M.G.L. and M.P.L conceived, designed, and implemented the project. M.P.L. and LCL carried out the experimental work and data collection. C.Y., O.B., R.N. carried out the data analysis. All authors were involved in interpretation of the data. M.P.L. and J.W. wrote the first draft of the manuscript, with subsequent contribution from all authors.

FUNDING

The work in M.G.L.'s lab was supported by an Australian Research Council (ARC) Discovery Program grant [DP220102840]; J.W. and L.C.L. were funded by an ARC Discovery Program grant [DP210103258]; J.W. is supported by a Kun Peng Fellowship from the Zhejiang Provincial government. Funding for open access charge: Zhejiang Provincial Government - Kun Peng Fellowship; Australian Research Council [DP210103258, DP220102840].

Conflict of interest statement. None declared.

REFERENCES

1. McSteen,P. and Kellogg,E.A. (2022) Molecular, cellular, and developmental foundations of grass diversity. *Science*, **377**, 599–602.
2. Wen,L., Li,G., Huang,T., Geng,W., Pei,H., Yang,J., Zhu,M., Zhang,P., Hou,R., Tian,G. *et al.* (2022) Single-cell technologies: from research to application. *Innovation (Camb)*, **3**, 100342.
3. Efroni,I., Mello,A., Nawy,T., Ip,P.L., Rahni,R., DelRose,N., Powers,A., Satija,R. and Birnbaum,K.D. (2016) Root regeneration triggers an embryo-like sequence guided by hormonal interactions. *Cell*, **165**, 1721–1733.
4. Denyer,T., Ma,X., Klesen,S., Scacchi,E., Nieselt,K. and Timmermans,M.C.P. (2019) Spatiotemporal developmental trajectories in the Arabidopsis root revealed using high-throughput single-cell RNA sequencing. *Dev. Cell*, **48**, 840–852.
5. Shulse,C.N., Cole,B.J., Ciobanu,D., Lin,J., Yoshinaga,Y., Gouran,M., Turco,G.M., Zhu,Y., O'Malley,R.C., Brady,S.M. *et al.* (2019) High-throughput single-cell transcriptome profiling of plant cell types. *Cell Rep.*, **27**, 2241–2247.
6. Liu,Z., Wang,J., Zhou,Y., Zhang,Y., Qin,A., Yu,X., Zhao,Z., Wu,R., Guo,C., Bawa,G. *et al.* (2022) Identification of novel regulators required for early development of vein pattern in the cotyledons by single-cell RNA-sequencing. *Plant J.*, **110**, 7–22.
7. Roszak,P., Heo,J.O., Blob,B., Toyokura,K., Sugiyama,Y., de Luis Balaguer,M.A., Lau,W.W.Y., Hamey,F., Cirrone,J., Madej,E. *et al.* (2021) Cell-by-cell dissection of phloem development links a maturation gradient to cell specialization. *Science*, **374**, eaba5531.
8. Tenorio Berrío,R., Verstaen,K., Vandamme,N., Pevernagie,J., Achon,I., Van Duyse,J., Van Isterdael,G., Saeys,Y., De Veylder,L., Inzé,D. *et al.* (2022) Single-cell transcriptomics sheds light on the identity and metabolism of developing leaf cells. *Plant Physiology*, **188**, 898–918.
9. Zhu,M., Taylor,I.W. and Benfey,P.N. (2022) Single-cell genomics revolutionizes plant development studies across scales. *Development*, **149**, dev200179.
10. Jha,S.G., Borowsky,A.T., Cole,B.J., Fahlgren,N., Farmer,A., Huang,S.C., Karia,P., Libault,M., Provart,N.J., Rice,S.L. *et al.* (2021) Vision, challenges and opportunities for a plant cell atlas. *Elife*, **10**, e66877.
11. Hafemeister,C. and Satija,R. (2019) Normalization and variance stabilization of single-cell RNA-seq data using regularized negative binomial regression. *Genome Biol.*, **20**, 296.
12. Kiselev,V.Y., Andrews,T.S. and Hemberg,M. (2019) Challenges in unsupervised clustering of single-cell RNA-seq data. *Nat. Rev. Genet.*, **20**, 273–282.
13. Cox,K.L., Gurazada,S.G.R., Duncan,K.E., Czymmek,K.J., Topp,C.N. and Meyers,B.C. (2022) Organizing your space: the

potential for integrating spatial transcriptomics and 3D imaging data in plants. *Plant Physiol.***188**, 703–712.
14. Giacomello,S. (2021) A new era for plant science: spatial single-cell transcriptomics. *Curr. Opin. Plant Biol.*, **60**, 102041.
15. Chen,S., Acosta,D., Li,L., Liang,J., Chang,Y., Wang,C., Fitzgerald,J., Morrison,C., Goulbourne,C.N., Nakano,Y. *et al.* (2022) Wolframin is a novel regulator of tau pathology and neurodegeneration. *Acta Neuropathol.*, **143**, 547–569.
16. Ben-Moshe,S., Veg,T., Manco,R., Dan,S., Papinutti,D., Lifshitz,A., Kolodziejczyk,A.A., Bahar Halpern,K., Elinav,E. and Itzkovitz,S. (2022) The spatiotemporal program of zonal liver regeneration following acute injury. *Cell Stem Cell*, **29**, 973–989.
17. Giacomello,S., Salmen,F., Terebieniec,B.K., Vickovic,S., Navarro,J.F., Alexeyenko,A., Reimegard,J., McKee,L.S., Mannapperuma,C., Bulone,V. *et al.* (2017) Spatially resolved transcriptome profiling in model plant species. *Nat Plants*, **3**, 17061.
18. Xia,K., Sun,H.X., Li,J., Li,J., Zhao,Y., Chen,L., Qin,C., Chen,R., Chen,Z., Liu,G. *et al.* (2022) The single-cell stereo-seq reveals region-specific cell subtypes and transcriptome profiling in Arabidopsis leaves. *Dev. Cell.***57**, 1299–1310.
19. Liu,C., Leng,J., Li,Y., Ge,T., Li,J., Chen,Y., Guo,C. and Qi,J. (2022) A spatiotemporal atlas of organogenesis in the development of orchid flowers. *Nucleic Acids Res.*, **50**, 9724–9737.
20. Du,J., Wang,Y.C., Chen,W., Xu,M., Zhou,R., Shou,H. and Chen,J. (2023) High-resolution anatomical and spatial transcriptome analyses reveal two types of meristematic cell pools within the secondary vascular tissue of poplar stem. *Mol Plant.***16**, 809–828.
21. Moreno-Villena,J.J., Zhou,H., Gilman,I.S., Tausta,S.L., Cheung,C.Y.M. and Edwards,E.J. (2022) Spatial resolution of an integrated C_4+CAM photosynthetic metabolism. *Science Advances*, **8**, eabn2349.
22. Lee,T.A., Nobori,T., Illouz-Eliaz,N., Xu,J., Jow,B., Nery,J.R. and Ecker,J.R. (2023) A single-nucleus atlas of seed-to-seed development in Arabidopsis. bioRxiv doi: https://doi.org/10.1101/2023.03.23.533992, 24 march 2023, preprint: not peer reviewed.
23. Song,X., Guo,P., Wang,M., Chen,L., Zhang,J., Xu,M., Liu,N., Liu,M., Fang,L., Xu,X. *et al.* (2023) Spatial transcriptomic atlas of shoot organogenesis in tomato callus. bioRxiv doi: https://doi.org/10.1101/2023.02.24.529793, 26 February 2023, preprint: not peer reviewed.
24. Giacomello,S. and Lundeberg,J. (2018) Preparation of plant tissue to enable Spatial transcriptomics profiling using barcoded microarrays. *Nat. Protoc.*, **13**, 2425–2446.
25. Mascher,M., Gundlach,H., Himmelbach,A., Beier,S., Twardziok,S.O., Wicker,T., Radchuk,V., Dockter,C., Hedley,P.E., Russell,J. *et al.* (2017) A chromosome conformation capture ordered sequence of the barley genome. *Nature*, **544**, 427–433.
26. Altenhoff,A.M., Train,C.M., Gilbert,K.J., Mediratta,I., Mendes de Farias,T., Moi,D., Nevers,Y., Radoykova,H.S., Rossier,V., Warwick Vesztrocy,A. *et al.* (2021) OMA orthology in 2021: website overhaul, conserved isoforms, ancestral gene order and more. *Nucleic Acids Res.*, **49**, D373–D379.
27. Miller,B.F., Bambah-Mukku,D., Dulac,C., Zhuang,X. and Fan,J. (2021) Characterizing spatial gene expression heterogeneity in spatially resolved single-cell transcriptomic data with nonuniform cellular densities. *Genome Res.*, **31**, 1843–1855.
28. Morabito,S., Reese,F., Rahimzadeh,N., Miyoshi,E. and Swarup,V. (2022) High dimensional co-expression networks enable discovery of transcriptomic drivers in complex biological systems. bioRxiv doi: https://doi.org/10.1101/2022.09.22.509094, 23 September 2022, preprint: not peer reviewed.
29. Ge,S.X., Jung,D. and Yao,R. (2019) ShinyGO: a graphical gene-set enrichment tool for animals and plants. *Bioinformatics*, **36**, 2628–2629.
30. Yu,G., Wang,L.G., Han,Y. and He,Q.Y. (2012) clusterProfiler: an R package for comparing biological themes among gene clusters. *OMICS*, **16**, 284–287.
31. Jackson,D.P. (1991) In: *Molecular Plant Pathology: A Practical Approach*. Oxford University Press, Vol. **1**.
32. Hao,Y., Hao,S., Andersen-Nissen,E., Mauck,W.M., Zheng,S., Butler,A., Lee,M.J., Wilk,A.J., Darby,C., Zager,M. *et al.* (2021) Integrated analysis of multimodal single-cell data. *Cell*, **184**, 3573–3587.
33. Becht,E., McInnes,L., Healy,J., Dutertre,C.A., Kwok,I.W.H., Ng,L.G., Ginhoux,F. and Newell,E.W. (2018) Dimensionality reduction for visualizing single-cell data using UMAP. *Nat. Biotechnol.***37**, 38–44.
34. Betts,N.S., Berkowitz,O., Liu,R., Collins,H.M., Skadhauge,B., Dockter,C., Burton,R.A., Whelan,J. and Fincher,G.B. (2017) Isolation of tissues and preservation of RNA from intact, germinated barley grain. *Plant J.*, **91**, 754–765.
35. Trapnell,C. (2015) Defining cell types and states with single-cell genomics. *Genome Res.*, **25**, 1491–1498.
36. Waddington,C.H. and Kacser,H. (1957) In: *The Strategy of the Genes: A Discussion of some Aspects of Theoretical Biology*. Allen & Unwin.
37. Kitanaga,Y., Jian,C., Hasegawa,M., Yazaki,J., Kishimoto,N., Kikuchi,S., Nakamura,H., Ichikawa,H., Asami,T., Yoshida,S. *et al.* (2006) Sequential regulation of gibberellin, brassinosteroid, and jasmonic acid biosynthesis occurs in rice coleoptiles to control the transcript levels of anti-microbial thionin genes. *Biosci. Biotechnol. Biochem.*, **70**, 2410–2419.
38. Sugimoto,N., Takeda,G., Nagato,Y. and Yamaguchi,J. (1998) Temporal and spatial expression of the α-amylase gene during seed germination in rice and barley. *Plant Cell Physiology*, **39**, 323–333.
39. Do,C.T., Pollet,B., Thévenin,J., Sibout,R., Denoue,D., Barrière,Y., Lapierre,C. and Jouanin,L. (2007) Both caffeoyl coenzyme A 3-O-methyltransferase 1 and caffeic acid O-methyltransferase 1 are involved in redundant functions for lignin, flavonoids and sinapoyl malate biosynthesis in Arabidopsis. *Planta*, **226**, 1117–1129.
40. Wei,K. and Zhong,X. (2014) Non-specific lipid transfer proteins in maize. *BMC Plant Biol.*, **14**, 281.
41. Gausing,K. (1994) Lipid transfer protein genes specifically expressed in barley leaves and coleoptiles. *Planta*, **192**, 574–580.
42. Hruz,T., Laule,O., Szabo,G., Wessendorp,F., Bleuler,S., Oertle,L., Widmayer,P., Gruissem,W. and Zimmermann,P. (2008) Genevestigator v3: a reference expression database for the meta-analysis of transcriptomes. *Adv. Bioinformatics*, **2008**, 420747.
43. Rajjou,L., Gallardo,K., Debeaujon,I., Vandekerckhove,J., Job,C. and Job,D. (2004) The effect of alpha-amanitin on the Arabidopsis seed proteome highlights the distinct roles of stored and neosynthesized mRNAs during germination. *Plant Physiol.*, **134**, 1598–1613.
44. Bai,B., van der Horst,S., Cordewener,J.H.G., America,T., Hanson,J. and Bentsink,L. (2020) Seed-stored mRNAs that are specifically associated to monosomes are translationally regulated during germination. *Plant Physiol.*, **182**, 378–392.
45. Ma,Z., Bykova,N.V. and Igamberdiev,A.U. (2017) Cell signaling mechanisms and metabolic regulation of germination and dormancy in barley seeds. *Crop J.*, **5**, 459–477.
46. Rylott,E.L., Gilday,A.D. and Graham,I.A. (2003) The gluconeogenic enzyme phosphoenolpyruvate carboxykinase in Arabidopsis is essential for seedling establishment. *Plant Physiol.*, **131**, 1834–1842.
47. Zhang,H., Sreenivasulu,N., Weschke,W., Stein,N., Rudd,S., Radchuk,V., Potokina,E., Scholz,U., Schweizer,P., Zierold,U. *et al.* (2004) Large-scale analysis of the barley transcriptome based on expressed sequence tags. *Plant J.*, **40**, 276–290.
48. Zhu,Y., Berkowitz,O., Selinski,J., Hartmann,A., Narsai,R., Wang,Y., Mao,P. and Whelan,J. (2020) Conserved and opposite transcriptome patterns during germination in Hordeum vulgare and Arabidopsis thaliana. *Int. J. Mol. Sci.*, **21**, 7404.
49. Narsai,R., Secco,D., Schultz,M.D., Ecker,J.R., Lister,R. and Whelan,J. (2017) Dynamic and rapid changes in the transcriptome and epigenome during germination and in developing rice (Oryza sativa) coleoptiles under anoxia and re-oxygenation. *Plant J.*, **89**, 805–824.
50. Law,S.R., Narsai,R. and Whelan,J. (2014) Mitochondrial biogenesis in plants during seed germination. *Mitochondrion*, **19**, 214–221.
51. CAMPBELL,S.A. and CLOSE,T.J. (1997) Dehydrins: genes, proteins, and associations with phenotypic traits. *New Phytologist*, **137**, 61–74.
52. D'Ovidio,R. and Masci,S. (2004) The low-molecular-weight glutenin subunits of wheat gluten. *J. Cereal Sci.*, **39**, 321–339.
53. Alfonso-Rubí,J., Ortego,F., Castañera,P., Carbonero,P. and Díaz,I. (2003) Transgenic expression of trypsin inhibitor CMe from barley

in indica and japonica rice, confers resistance to the rice weevil Sitophilus oryzae. *Transgenic Res.*, **12**, 23–31.
54. Iqbal,I., Tripathi,R.K., Wilkins,O. and Singh,J. (2020) Thaumatin-like protein (TLP) gene Family in Barley: genome-wide exploration and expression analysis during germination. *Genes (Basel)*, **11**, 1080.
55. Topham,A.T., Taylor,R.E., Yan,D., Nambara,E., Johnston,I.G. and Bassel,G.W. (2017) Temperature variability is integrated by a spatially embedded decision-making center to break dormancy in *Arabidopsis* seeds. *Proc. Natl. Acad. Sci. U.S.A.*, **114**, 6629–6634.
56. Holloway,T., Steinbrecher,T., Perez,M., Seville,A., Stock,D., Nakabayashi,K. and Leubner-Metzger,G. (2021) Coleorhiza-enforced seed dormancy: a novel mechanism to control germination in grasses. *New Phytol.*, **229**, 2179–2191.
57. Barrero,J.M., Talbot,M.J., White,R.G., Jacobsen,J.V. and Gubler,F. (2009) Anatomical and transcriptomic studies of the Coleorhiza reveal the importance of this tissue in regulating dormancy in Barley. *Plant Physiol.*, **150**, 1006–1021.
58. Bewley,J.D. (1997) Seed germination and dormancy. *Plant Cell*, **9**, 1055–1066.
59. Weitbrecht,K., Müller,K. and Leubner-Metzger,G. (2011) First off the mark: early seed germination. *J. Exp. Bot.*, **62**, 3289–3309.
60. Footitt,S., Clewes,R., Feeney,M., Finch-Savage,W.E. and Frigerio,L. (2019) Aquaporins influence seed dormancy and germination in response to stress. *Plant Cell Environ.*, **42**, 2325–2339.
61. Hoai,P.T.T., Tyerman,S.D., Schnell,N., Tucker,M., McGaughey,S.A., Qiu,J., Groszmann,M. and Byrt,C.S. (2020) Deciphering aquaporin regulation and roles in seed biology. *J. Exp. Bot.*, **71**, 1763–1773.
62. Richard,J.A., Kelly,I., Marion,D., Pézolet,M. and Auger,M. (2002) Interaction between beta-purothionin and dimyristoylphosphatidylglycerol: a (31)P-NMR and infrared spectroscopic study. *Biophys. J.*, **83**, 2074–2083.
63. Rösti,J., Barton,C.J., Albrecht,S., Dupree,P., Pauly,M., Findlay,K., Roberts,K. and Seifert,G.J. (2007) UDP-glucose 4-epimerase isoforms UGE2 and UGE4 cooperate in providing UDP-galactose for cell wall biosynthesis and growth of *Arabidopsis thaliana*. *Plant Cell*, **19**, 1565–1579.
64. Oard,S. and Karki,B. (2006) Mechanism of beta-purothionin antimicrobial peptide inhibition by metal ions: molecular dynamics simulation study. *Biophys. Chem.*, **121**, 30–43.
65. Qi,P.F., Wei,Y.M., Ouellet,T., Chen,Q., Tan,X. and Zheng,Y.L. (2009) The gamma-gliadin multigene family in common wheat (Triticum aestivum) and its closely related species. *BMC Genomics*, **10**, 168.
66. Park,E.J. and Kim,T.H. (2021) Arabidopsis OSMOTIN 34 functions in the ABA signaling pathway and is regulated by proteolysis. *Int. J. Mol. Sci.*, **22**, 7915.
67. Ren,Y., Liu,Y., Chen,H., Li,G., Zhang,X. and Zhao,J. (2012) Type 4 metallothionein genes are involved in regulating Zn ion accumulation in late embryo and in controlling early seedling growth in Arabidopsis. *Plant Cell Environ.*, **35**, 770–789.
68. Wang,Y., Zhao,Z., Liu,F., Sun,L. and Hao,F. (2020) Versatile roles of aquaporins in plant growth and development. *Int. J. Mol. Sci.*, **21**, 9485.
69. Maurel,C., Verdoucq,L., Luu,D.T. and Santoni,V. (2008) Plant aquaporins: membrane channels with multiple integrated functions. *Annu. Rev. Plant Biol.*, **59**, 595–624.
70. Liu,C., Fukumoto,T., Matsumoto,T., Gena,P., Frascaria,D., Kaneko,T., Katsuhara,M., Zhong,S., Sun,X., Zhu,Y. *et al.* (2013) Aquaporin OsPIP1;1 promotes rice salt resistance and seed germination. *Plant Physiol. Biochem.*, **63**, 151–158.
71. Ding,L., Uehlein,N., Kaldenhoff,R., Guo,S., Zhu,Y. and Kai,L. (2019) Aquaporin PIP2;1 affects water transport and root growth in rice (*Oryza sativa* L.). *Plant Physiol. Biochem.*, **139**, 152–160.
72. Knipfer,T., Besse,M., Verdeil,J.L. and Fricke,W. (2011) Aquaporin-facilitated water uptake in barley (Hordeum vulgare L.) roots. *J. Exp. Bot.*, **62**, 4115–4126.
73. Maurel,C., Reizer,J., Schroeder,J.I. and Chrispeels,M.J. (1993) The vacuolar membrane protein gamma-TIP creates water specific channels in *Xenopus oocytes*. *EMBO J.*, **12**, 2241–2247.
74. Regon,P., Panda,P., Kshetrimayum,E. and Panda,S.K. (2014) Genome-wide comparative analysis of tonoplast intrinsic protein (TIP) genes in plants. *Funct. Integr. Genomics*, **14**, 617–629.
75. Utsugi,S., Shibasaka,M., Maekawa,M. and Katsuhara,M. (2015) Control of the water transport activity of Barley HvTIP3;1 specifically expressed in seeds. *Plant Cell Physiology*, **56**, 1831–1840.
76. Haferkamp,I., Fernie,A.R. and Neuhaus,H.E. (2011) Adenine nucleotide transport in plants: much more than a mitochondrial issue. *Trends Plant Sci.*, **16**, 507–515.
77. BRISKIN,D.P. and HANSON,J.B. (1992) How does the plant plasma membrane H+-atpase pump protons?*J. Exp. Bot.*, **43**, 269–289.
78. Enríquez-Arredondo,C., Sánchez-Nieto,S., Rendón-Huerta,E., González-Halphen,D., Gavilanes-Ruíz,M. and Díaz-Pontones,D. (2005) The plasma membrane H+-atpase of maize embryos localizes in regions that are critical during the onset of germination. *Plant Sci.*, **169**, 11–19.
79. Li,H., Li,X., Wang,G., Zhang,J. and Wang,G. (2022) Analysis of gene expression in early seed germination of rice: landscape and genetic regulation. *BMC Plant Biol.*, **22**, 70.
80. Mundy,J. (1984) Hormonal regulation of α-amylase inhibitor synthesis in germinating barley. *Carlsberg Res. Commun.*, **49**, 439–444.
81. Collins,H.M., Betts,N.S., Dockter,C., Berkowitz,O., Braumann,I., Cuesta-Seijo,J.A., Skadhauge,B., Whelan,J., Bulone,V. and Fincher,G.B. (2021) Genes that mediate starch metabolism in developing and germinated barley grain. *Front. Plant Sci.*, **12**, 641325.
82. Franco,O.L., Rigden,D.J., Melo,F.R. and Grossi-De-Sa,M.F. (2002) Plant alpha-amylase inhibitors and their interaction with insect alpha-amylases. *Eur. J. Biochem.*, **269**, 397–412.
83. Damaris,R.N., Lin,Z., Yang,P. and He,D. (2019) The rice alpha-amylase, conserved regulator of seed maturation and germination. *Int. J. Mol. Sci.*, **20**, 450.
84. Goswami,A.K., Jain,M.K. and Paul,B. (1977) α- and β-amylases in seed germination. *Biologia Plantarum*, **19**, 469–471.
85. Gendreau,E., Romaniello,S., Barad,S., Leymarie,J., Benech-Arnold,R. and Corbineau,F. (2008) Regulation of cell cycle activity in the embryo of barley seeds during germination as related to grain hydration. *J. Exp. Bot.*, **59**, 203–212.
86. Barrôco,R.M., Van Poucke,K., Bergervoet,J.H., De Veylder,L., Groot,S.P., Inzé,D. and Engler,G. (2005) The role of the cell cycle machinery in resumption of postembryonic development. *Plant Physiol.*, **137**, 127–140.
87. Wolny,E., Betekhtin,A., Rojek,M., Braszewska-Zalewska,A., Lusinska,J. and Hasterok,R. (2018) Germination and the early stages of seedling development in Brachypodium distachyon. *Int. J. Mol. Sci.*, **19**, 2916.
88. An,Y.Q. and Lin,L. (2011) Transcriptional regulatory programs underlying barley germination and regulatory functions of gibberellin and abscisic acid. *BMC Plant Biol.*, **11**, 105.
89. Li,Y., Jones,L. and McQueen-Mason,S. (2003) Expansins and cell growth. *Curr. Opin. Plant Biol.*, **6**, 603–610.
90. Zhang,Q., Hrmova,M., Shirley,N.J., Lahnstein,J. and Fincher,G.B. (2006) Gene expression patterns and catalytic properties of UDP-D-glucose 4-epimerases from barley (Hordeum vulgare L.). *Biochem. J.*, **394**, 115–124.
91. Flematti,G.R., Dixon,K.W. and Smith,S.M. (2015) What are karrikins and how were they 'discovered' by plants?*BMC Biology*, **13**, 108.
92. Zhu,H., Xie,W., Xu,D., Miki,D., Tang,K., Huang,C.F. and Zhu,J.K. (2018) DNA demethylase ROS1 negatively regulates the imprinting of DOGL4 and seed dormancy in Arabidopsis thaliana. *Proc. Natl. Acad. Sci. U.S.A.*, **115**, E9962–E9970.
93. Osnato,M., Stile,M.R., Wang,Y., Meynard,D., Curiale,S., Guiderdoni,E., Liu,Y., Horner,D.S., Ouwerkerk,P.B., Pozzi,C. *et al.* (2010) Cross talk between the KNOX and ethylene pathways is mediated by intron-binding transcription factors in barley. *Plant Physiol.*, **154**, 1616–1632.
94. Dirk,L.M.A., Kumar,S., Majee,M. and Downie,A.B. (2018) PHYTOCHROME INTERACTING FACTOR1 interactions leading to the completion or prolongation of seed germination. *Plant Signal Behav*, **13**, e1525999.
95. Yang,L., Jiang,Z., Jing,Y. and Lin,R. (2020) PIF1 and RVE1 form a transcriptional feedback loop to control light-mediated seed germination in Arabidopsis. *J. Integr. Plant Biol.*, **62**, 1372–1384.

96. Zhang,M., Liu,W. and Bi,Y.P. (2009) (Dehydration-responsive element-binding (DREB) transcription factor in plants and its role during abiotic stresses). *Yi Chuan*, **31**, 236–244.
97. Schmal,C., Myung,J., Herzel,H. and Bordyugov,G. (2017) Moran's I quantifies spatio-temporal pattern formation in neural imaging data. *Bioinformatics*, **33**, 3072–3079.
98. Svensson,V., Teichmann,S.A. and Stegle,O. (2018) SpatialDE: identification of spatially variable genes. *Nat. Methods*, **15**, 343–346.
99. Yano,R., Takebayashi,Y., Nambara,E., Kamiya,Y. and Seo,M. (2013) Combining association mapping and transcriptomics identify HD2B histone deacetylase as a genetic factor associated with seed dormancy in Arabidopsis thaliana. *Plant J.*, **74**, 815–828.
100. Wang,Z., Chen,F., Li,X., Cao,H., Ding,M., Zhang,C., Zuo,J., Xu,C., Xu,J., Deng,X. *et al.* (2016) Arabidopsis seed germination speed is controlled by SNL histone deacetylase-binding factor-mediated regulation of AUX1. *Nat. Commun.*, **7**, 13412.
101. Wang,Z., Cao,H., Sun,Y., Li,X., Chen,F., Carles,A., Li,Y., Ding,M., Zhang,C., Deng,X. *et al.* (2013) Arabidopsis paired amphipathic helix proteins SNL1 and SNL2 redundantly regulate primary seed dormancy via abscisic acid-ethylene antagonism mediated by histone deacetylation. *Plant Cell*, **25**, 149–166.
102. Jin,J., Hewezi,T. and Baum,T.J. (2011) The Arabidopsis bHLH25 and bHLH27 transcription factors contribute to susceptibility to the cyst nematode Heterodera schachtii. *Plant J.*, **65**, 319–328.
103. Rubinovich,L. and Weiss,D. (2010) The Arabidopsis cysteine-rich protein GASA4 promotes GA responses and exhibits redox activity in bacteria and in planta. *Plant J.*, **64**, 1018–1027.
104. Roxrud,I., Lid,S.E., Fletcher,J.C., Schmidt,E.D. and Opsahl-Sorteberg,H.G. (2007) GASA4, one of the 14-member Arabidopsis GASA family of small polypeptides, regulates flowering and seed development. *Plant Cell Physiol.*, **48**, 471–483.
105. Zhong,C., Xu,H., Ye,S., Wang,S., Li,L., Zhang,S. and Wang,X. (2015) Gibberellic acid-stimulated Arabidopsis6 serves as an integrator of gibberellin, abscisic acid, and glucose signaling during seed germination in Arabidopsis. *Plant Physiol.*, **169**, 2288–2303.
106. Vernoux,T., Wilson,R.C., Seeley,K.A., Reichheld,J.P., Muroy,S., Brown,S., Maughan,S.C., Cobbett,C.S., Van Montagu,M., Inzé,D. *et al.* (2000) The ROOT MERISTEMLESS1/CADMIUM SENSITIVE2 gene defines a glutathione-dependent pathway involved in initiation and maintenance of cell division during postembryonic root development. *Plant Cell*, **12**, 97–110.
107. Bashandy,T., Guilleminot,J., Vernoux,T., Caparros-Ruiz,D., Ljung,K., Meyer,Y. and Reichheld,J.P. (2010) Interplay between the NADP-linked thioredoxin and glutathione systems in Arabidopsis auxin signaling. *Plant Cell*, **22**, 376–391.
108. Koprivova,A., Mugford,S.T. and Kopriva,S. (2010) Arabidopsis root growth dependence on glutathione is linked to auxin transport. *Plant Cell Rep.*, **29**, 1157–1167.
109. Liew,L.C., Narsai,R., Wang,Y., Berkowitz,O., Whelan,J. and Lewsey,M.G. (2020) Temporal tissue-specific regulation of transcriptomes during barley (Hordeum vulgare) seed germination. *Plant J.*, **101**, 700–715.
110. Narsai,R., Gouil,Q., Secco,D., Srivastava,A., Karpievitch,Y.V., Liew,L.C., Lister,R., Lewsey,M.G. and Whelan,J. (2017) Extensive transcriptomic and epigenomic remodelling occurs during Arabidopsis thaliana germination. *Genome Biol.*, **18**, 172.
111. Yang,J., Su,L., Li,D., Luo,L., Sun,K., Yang,M., Gu,F., Xia,A., Liu,Y., Wang,H. *et al.* (2020) Dynamic transcriptome and metabolome analyses of two types of rice during the seed germination and young seedling growth stages. *BMC Genomics*, **21**, 603.
112. Dresselhaus,T. and Jürgens,G. (2021) Comparative embryogenesis in angiosperms: activation and patterning of embryonic cell lineages. *Annu. Rev. Plant Biol.*, **72**, 641–676.
113. Du,Y. and Scheres,B. (2018) Lateral root formation and the multiple roles of auxin. *J. Exp. Bot.*, **69**, 155–167.
114. Feng,Y., Bayaer,E. and Qi,Y. (2022) Advances in the biological functions of auxin transporters in rice. *Agriculture*, **12**, 1–17.
115. Möller,B. and Weijers,D. (2009) Auxin control of embryo patterning. *Cold Spring Harb. Perspect. Biol.*, **1**, a001545.
116. Abley,K. and Locke,J.C.W. (2021) Noisy transcription under the spotlight. *Nat Plants*, **7**, 996–997.
117. Asp,M., Bergenstråhle,J. and Lundeberg,J. (2020) Spatially resolved transcriptomes-next generation tools for tissue exploration. *Bioessays*, **42**, e1900221.
118. van den Berg,T., Yalamanchili,K., de Gernier,H., Santos Teixeira,J., Beeckman,T., Scheres,B., Willemsen,V. and Ten Tusscher,K. (2021) A reflux-and-growth mechanism explains oscillatory patterning of lateral root branching sites. *Dev. Cell*, **56**, 2176–2191.
119. Perianez-Rodriguez,J., Rodriguez,M., Marconi,M., Bustillo-Avendaño,E., Wachsman,G., Sanchez-Corrionero,A., De Gernier,H., Cabrera,J., Perez-Garcia,P., Gude,I. *et al.* (2021) An auxin-regulable oscillatory circuit drives the root clock in Arabidopsis. *Sci. Adv.*, **7**, eabd4722.
120. Leftley,N., Banda,J., Pandey,B., Bennett,M. and Voß,U. (2021) Uncovering how Auxin optimizes root systems architecture in response to environmental stresses. *Cold Spring Harb. Perspect. Biol.*, **13**, a040014.
121. Mehra,P., Pandey,B.K., Melebari,D., Banda,J., Leftley,N., Couvreur,V., Rowe,J., Anfang,M., De Gernier,H., Morris,E. *et al.* (2022) Hydraulic flux-responsive hormone redistribution determines root branching. *Science*, **378**, 762–768.
122. Péret,B., Li,G., Zhao,J., Band,L.R., Voß,U., Postaire,O., Luu,D.T., Da Ines,O., Casimiro,I., Lucas,M. *et al.* (2012) Auxin regulates aquaporin function to facilitate lateral root emergence. *Nat. Cell Biol.*, **14**, 991–998.
123. Panchy,N., Lehti-Shiu,M. and Shiu,S.H. (2016) Evolution of gene duplication in plants. *Plant Physiol.*, **171**, 2294–2316.
124. Fiorucci,A.S. (2020) To grow or defend? More on the plant cornelian dilemma. *Plant Physiol.*, **183**, 437–438.
125. Major,I.T., Guo,Q., Zhai,J., Kapali,G., Kramer,D.M. and Howe,G.A. (2020) A phytochrome B-independent pathway restricts growth at high levels of jasmonate defense. *Plant Physiol.*, **183**, 733–749.
126. Zandalinas,S.I. and Mittler,R. (2021) Vascular and nonvascular transmission of systemic reactive oxygen signals during wounding and heat stress. *Plant Physiol.*, **186**, 1721–1733.
127. Xu,Y., Zhang,X., Li,H., Zheng,H., Zhang,J., Olsen,M.S., Varshney,R.K., Prasanna,B.M. and Qian,Q. (2022) Smart breeding driven by big data, artificial intelligence, and integrated genomic-enviromic prediction. *Mol Plant*, **15**, 1664–1695.
128. Mackenzie,S.A. and Mullineaux,P.M. (2022) Plant environmental sensing relies on specialized plastids. *J. Exp. Bot.*, **73**, 7155–7164.
129. Betts,N.S., Dockter,C., Berkowitz,O., Collins,H.M., Hooi,M., Lu,Q., Burton,R.A., Bulone,V., Skadhauge,B., Whelan,J. *et al.* (2020) Transcriptional and biochemical analyses of gibberellin expression and content in germinated barley grain. *J. Exp. Bot.*, **71**, 1870–1884.
130. Sreenivasulu,N., Usadel,B., Winter,A., Radchuk,V., Scholz,U., Stein,N., Weschke,W., Strickert,M., Close,T.J., Stitt,M. *et al.* (2008) Barley grain maturation and germination: metabolic pathway and regulatory network commonalities and differences highlighted by new MapMan/PageMan profiling tools. *Plant Physiol.*, **146**, 1738–1758.
131. Cheng,M., Jiang,Y., Xu,J., Mentis,A.A., Wang,S., Zheng,H., Sahu,S.K., Liu,L. and Xu,X. (2023) Spatially resolved transcriptomics: a comprehensive review of their technological advances, applications, and challenges. *J. Genet. Genomics.*, **50**, 151–162.
132. Vandereyken,K., Sifrim,A., Thienpont,B. and Voet,T. (2023) Methods and applications for single-cell and spatial multi-omics. *Nat. Rev. Genet.*, 1–22.